Astronomy & Astrophysics manuscript no. non_detect_v6.3.1_arXiv
March 16, 2016
©ESO 2016

A coronagraphic search for wide sub-stellar companions among members of the Ursa Major moving group⋆ *(Research Note)*

M. Ammler - von Eiff[1,2,3,4,5,6], A. Bedalov[3,7], C. Kranhold[2], M. Mugrauer[3], T.O.B. Schmidt[3,8], R. Neuhäuser[3], and R. Errmann[3,9]

[1] Max-Planck-Institut für Sonnensystemforschung, Justus-von-Liebig-Weg 3, 37077 Göttingen, Germany, e-mail: ammler@mps.mpg.de
[2] Thüringer Landessternwarte, Sternwarte 5, 07778 Tautenburg, Germany
[3] Astrophysikalisches Institut und Universitäts-Sternwarte Jena, Schillergäßchen 2-3, 07745 Jena, Germany
[4] Centro de Astronomia e Astrofísica da Universidade de Lisboa, Observatório Astronómico de Lisboa, Tapada da Ajuda, 1349-018 Lisboa, Portugal
[5] Centro de Astrofísica da Universidade do Porto, Rua das Estrelas, 4150-762 Porto, Portugal
[6] Georg-August-Universität, Institut für Astrophysik. Friedrich-Hund-Platz 1, 37077 Göttingen, Germany
[7] Faculty of Natural Sciences, University of Split, Teslina 12. 21000 Split, Croatia
[8] Hamburger Sternwarte, Gojenbergsweg 112, 21029 Hamburg, Germany
[9] Abbe Center of Photonics, Friedrich-Schiller-Universität Jena, Max-Wien-Platz 1, 07743 Jena, Germany

arXiv:1603.04616v1 [astro-ph.SR] 15 Mar 2016

ABSTRACT

Context. We present the results of a survey to detect low-mass companions of UMa group members, carried out in 2003-2006 with NACO at the ESO VLT. While many extra-solar planets and planetary candidates have been found in close orbits around stars by the radial velocity and the transit method, direct detections at wider orbits are rare. The Ursa Major (UMa) group, a young stellar association at an age of about 200-600 Myr and an average distance of 25 pc, has not yet been addressed as a whole although its members represent a very interesting sample to search for and characterize sub-stellar companions by direct imaging.
Aims. Our goal was to find or to provide detection limits on wide sub-stellar companions around nearby UMa group members using high-resolution imaging.
Methods. We searched for faint companions around 20 UMa group members within 30 pc. The primaries were placed below a semi-transparent coronagraph, a rather rarely used mode of NACO, to increase the dynamic range of the images. In most cases, second epoch images of companion candidates were taken to check whether they share common proper motion with the primary.
Results. Our coronagraphic images rule out sub-stellar companions around the stars of the sample. A dynamical range of typically 13-15 mag in the K_s band was achieved at separations beyond 3" from the star. Candidates as faint as $K_s \approx 20$ were securely identified and measured. The survey is most sensitive between separations of 100 and 200 au but only on average because of the very different target distance. Field coverage reaches about 650 au for the most distant targets. Most of the 200 candidates are visible in two epochs. All of those were rejected being distant background objects.

Key words. Stars: binaries: visual – Stars: imaging – Stars: brown dwarfs – Galaxy: open clusters and associations: individual: UMa group – Galaxy: solar neighborhood

1. Introduction

By now almost 1,300 brown dwarfs have been found, classified with spectral types L, T, and Y (Kirkpatrick 2008; Cushing et al. 2011)[1]. This number has been surpassed by indirect detections in the planetary regime – by now more than 600 by radial velocity variations and more than 1,200 by the transit method.[2]

While indirect methods are most sensitive to objects in very close orbits around the targets, direct imaging detects objects in wider orbits and thus is complementary. Ideally, direct imaging is combined with simultaneous measurement of the radial velocity variation (Guenther et al. 2005). Young sub-stellar objects still contract and are self-luminous (Burrows et al. 1997) so that their direct detection is less difficult up to ages of a few hundred Myr (Malkov et al. 1998; Neuhäuser & Schmidt 2012). In contrast to high-resolution imaging in space (e.g. Marengo et al. 2006), ground-based observations need to encompass the seeing which can be done with adaptive optics (e.g. Neuhäuser et al. 2003; Duchêne et al. 2007). Coronagraphy with intransparent (e.g. McCarthy & Zuckerman 2004, Chauvin et al. 2005) or semi-transparent coronagraphs (e.g. Biller et al. 2010; Boccaletti et al. 2013, Guenther et al. 2005; Itoh et al. 2006, 2008a; Neuhäuser et al. 2007, Wahhaj et al. 2011) shade the bright star so that the exposure time and thus the sensitivity of the images can be increased. A number of very sophisticated techniques have been developed recently (see the review by Fischer et al. 2014).

Send offprint requests to: M. Ammler - von Eiff

⋆ Based on observations collected at the European Southern Observatory, Chile, in programmes 72.C-0485, 73.C-0225, 76.C-0777, 77.C-0268, 384.C-0245A

[1] See http://www.DwarfArchives.org for a full account.
[2] See http://www.exoplanet.eu for further details and updates.

The frequency of low-mass companions to stars gives important clues regarding our understanding of the formation of brown dwarfs and planets (Ida & Lin 2004; Alibert et al. 2005; Broeg 2007). At wide orbits, where direct imaging surveys are sensitive, the frequency of brown dwarfs is of the order of several percent for host stars with spectral types A-M and is less constrained for giant planets (Rameau et al. 2013; Bowler et al. 2015). In young nearby associations Neuhäuser & Guenther (2004) measure a frequency of 6 ± 4 % of sub-stellar companions which is not very different from the value of 1 ± 1 % obtained for isolated late-type stars (McCarthy & Zuckerman 2004). The frequency of brown dwarfs around Hyades members does not turn out very different from the latter (Guenther et al. 2005; Bouvier et al. 2008, Lodieu et al. 2014) although the Hyades are still young with an age of ≈600 Myr. In the younger Pleiades (125 Myr), Yamamoto et al. (2013) confirmed two brown dwarf companions in a sample of 20 stars.

Young moving groups of an age intermediate between the Pleiades and the Hyades offer interesting opportunities to study homogeneous samples of common age and origin. No sub-stellar companions have been found in the Her-Lyr assiociation (Eisenbeiss et al. 2007, Biller et al. 2013) which has an age of ≈250 Myr, similar to the UMa group (Eisenbeiss et al. 2013). Although a systematic survey of the UMa group at high resolution has been missing, low-mass companions have been detected: GJ 569 Ba, Bb (Martín et al. 2000; Zapatero Osorio et al. 2004), HD 130948 B & C, (Potter et al. 2002), and χ^1 Ori B (König et al. 2002)[3]. The only known planet around a probable UMa group member, ϵ Eri, was found by radial velocity variations (Hatzes et al. 2000; Benedict et al. 2006). Although there are still doubts about its existence (Zechmeister et al. 2013), there are even suspections of a second planet (Quillen & Thorndike 2002; Deller & Maddison 2005). The planet(s) of ϵ Eri have been subject to many, yet unsuccessful, attempts of direct detection (Itoh et al. 2006; Janson et al. 2007; Marengo et al. 2006; Neuhäuser & Schmidt 2012, and the present work).

The goal of the present work is to find additional sub-stellar companions in the UMa group by direct imaging. The search for close and faint companions in the UMa group benefits from a relatively young age of 200-600 Myrs [4], the small distance of members (≈50 pc on average; Fig. 1), and thus the availability of precise Hipparcos astrometry (Perryman et al. 1997; van Leeuwen 2007). Furthermore, the proper motion of UMa group members is high on average (≈50 mas/yr) because of their proximity (Fig. 1) and their peculiar space motion (Ammler 2006). Hence, co-moving companions can be identified already after a short epoch difference. Preliminary results of the present study have been published earlier (Ammler-von Eiff et al. 2009).

2. Coronagraphic observations and data reduction

As the definition of the UMa group and the list of members is controversial, we compiled the targets in the following way to get a meaningful number of reliable UMa group members closer than 30 pc and observable with NACO at the ESO VLT:

- stars found by Montes et al. (2001) to fulfil at least one of Eggen's kinematic criteria (Eggen 1995).
- certain or probable members compiled by King et al. (2003) based on photometric, kinematic, and spectroscopic criteria.
- HD 135599 which is an UMa group member according to Fuhrmann (2004).

One system, GJ 569 (=HIP 72944), we did not observe since it has been extensively studied before (e.g. Simon et al. 2006). Some objects were excluded because of known bright secondaries in the field of view (HD 24916, HD 29875, HD 98712, and HD 134083). HIP 104383 A is a close binary, too, but fully fits below the coronagraph so that we did observe it (Fig. D.1), i.e. 20 targets in total (Tables A.1 and A.2).

The targets have been observed with NACO, the adaptive optics imager at the Nasmyth platform of the ESO VLT UT4 (Yepun)[5]. The stars themselves were used as adaptive optics reference stars for the visual wavefront sensor of NAOS (VIS). First epoch images were taken in 2003/2004 (programmes 072.C-0485, 073.C-0225) and second epoch imaging followed in 2005/2006 (programmes 076.C-777, 077.C-0268) for those stars with faint companion candidates identified.

The semi-transparent coronagraph is a rarely used NACO mode. It has a diameter of 0.″7 and dims the incoming stellar light by about 6 magnitudes in the K band (see Fig. 1). Hence, it blocks most light of the star but still allows one to do precise astrometry with the stellar point spread function (PSF).

The observations have been obtained in the K_s band (Persson et al. 1998; Tokunaga et al. 2002) further reducing the brightness difference of stars and any low-mass companions. The sensitivity of the observations has been further improved by not using the S13 camera with the smallest pixel scale but instead observing with the S27 camera (27.15 mas/pix, FOV 28"x28").

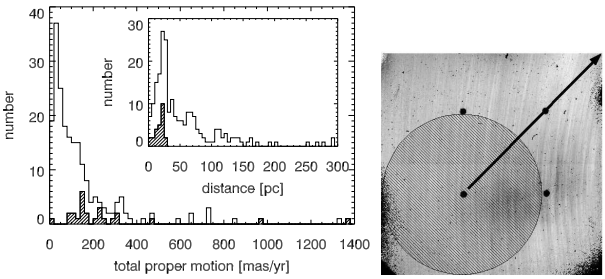

Fig. 1. Left: distribution of distance and proper motion. The major concentration of the UMa group is the UMa open cluster in the Big Dipper constellation at distances of about 25 pc. All known members and candidates (see references in the text) are included in the histogram (solid line; distances mostly from Montes et al. 2001 and van Leeuwen 2007). We add the distribution of the southern stars within 30 pc addressed in the present work (hatched; distances from van Leeuwen 2007). Right: an image of the coronagraphic mask with the four coronagraphs (black filled circles) taken with the S27 camera. Each of the coronagraphs has an angular diameter of 0.″7. We placed the star below the lower left (south-eastern) coronagraph, so that a field with a radius of ≈9" is completely covered outside the coronagraph (hatched circle). Incomplete coverage is achieved up to separations of ≈25" (arrow).

[3] It is worth noting that Bannister & Jameson (2007) identified one T dwarf and three L dwarfs in the UMa group using the moving cluster method.

[4] The Ursa Major (UMa) has been studied extensively under various aspects (e.g. Eggen 1994; Montes et al. 2001; King et al. 2003; Fuhrmann 2004; Ammler 2006) but the precise age and the list of members are still a matter of debate. Age estimates range from 200 to 600 Myrs (König et al. 2002; King et al. 2003; Fuhrmann 2004; King & Schuler 2005; Brandt & Huang 2015).

[5] NACO consists of the adaptive optics system NAOS (Lenzen et al. 2003) and the camera CONICA (Rousset et al. 2003). The instrument was decommissioned in August 2013 and recommissioned on UT1 in January 2015.

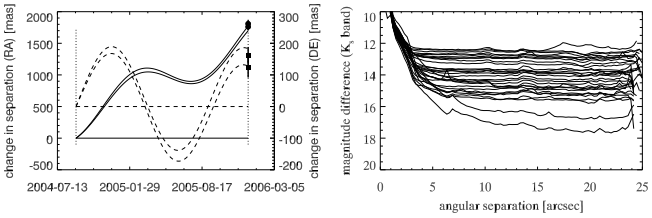

Fig. 2. Left: based on Hipparcos data (cf. Tables E.2, A.1, and A.2), this example of HD 22049 shows how the relative motion of non-moving background stars in right ascension (solid lines) and declination (dashed lines) will differ from a comoving companion (respective horizontal lines). The lines encompass the Hipparcos uncertainty, scaled by a factor of 100 for visibility. Possible orbital motion of a hypothetical companion has been neglected. The vertical dotted lines highlight the dates of the 1st and 2nd epoch exposures, respectively. Obviously, the two candidates found are background objects (circles for right ascension and squares for declination, resp.; see Table D.2 and Fig. C.1). Right: dynamic range curves for a $10\,\sigma$ detection as a function of angular separation for all exposures of the survey.

This way, a larger field is covered (Fig. 1) and more light is collected in a single pixel. The astrometric precision using the S27 camera is sufficient since the average proper motion of the UMa group of 150 mas (Fig. 1) per year corresponds to 5.5 pixels on the detector.

The data reduction follows the usual steps of sky subtraction, flat-field correction, bad pixel correction, shift and add[6]. The sky has been subtracted using jittered exposures of nearby sky positions free of bright stars. The flat-field correction is based on coronagraphic night-time flat-field exposures to correct for the variable transmittance of the coronagraphic substrate and standard day-time exposures to correct for pixel-to-pixel variations of the detector below the coronagraph used. Bad pixel frames have been taken from standard calibrations or derived individually with ESO tools and standard twilight flat-field exposures.

3. Identification and characterisation of candidates

The stellar PSF has been subtracted in a box of 500x500 pixels centred on the star to facilitate the visual identification of faint companion candidates. The PSF has been derived by calculating the average of a set of rotated frames (in steps of 2°) and using sigma-clipping to get rid of bright features, in particular the diffraction spikes. A smoothed image has been subtracted to further facilitate detection (Figs C.1-C.5)[7].

We noticed that artefacts due to dust particles on the coronagraphic substrate can be mistaken for companion candidates. The flat-field correction fails in removing those since occasional displacements of the coronagraphic substrate can occur between calibration and target exposures. We removed those artefacts from the list of companion candidates guided by a visual cross-match of the scientific exposures with the flat-field exposures. In the most extreme cases (exposures of HD 11171 and HD 22049), several tens of artefacts had to be removed.

[6] using own scripts and tools provided by ESO, including *ESO-eclipse* v5.0.0, the *jitter* recipe (Devillard 1997, 2011), and *esorex* using the recipe *naco_img_twflat* to derive bad pixel frames.

[7] Smoothing has been done by the application of a Gaussian filter (*FILTER/GAUSS* in ESO MIDAS version 13SEP; Banse et al. 1983; Warmels 1992) using all adjacent pixels within a radius of 18 pixels weighted by a Gaussian with a width of $\sigma = 3$ pixels.

A wide comoving companion will not change its position relative to the star while a distant and thus non-moving background object will reflect the stellar parallactic and proper motion (Fig. 2). Our assessment of astrometric measurement uncertainties is based on Chauvin et al. (2010) who give a long-term average of the S27 pixel scale of 27.012 ± 0.004 mas/pix and of the detector position angle (true North) of $-0.^\circ04 \pm 0.^\circ14$. In the present work, we corrected the position angles of all candidates for the mean deviation of $-0.^\circ04$ from the true North. From the measurements obtained by Chauvin et al. (2010), we expect uncertainties of 0.016 mas/pix on separation and $0.^\circ15$ on position angle. We neglected the errors in fitting Gaussian profiles to measure the positions of the stars and the candidates. It is as precise as a few milliarcseconds and of the order of the *Hipparcos* errors (Table E.2).

The instrumental magnitudes of the target stars and the candidates have all been measured in apertures of 13 pixels across which is more than double the typical FWHM of the PSF. Then, the K_s band magnitude of the candidates has been derived from the measured flux ratios taking into account the brightness of the target star (Table A.2) and the attenuation of the coronagraph. While the brightness of the star has been measured in the reduced frames, the brightness of the candidates has been measured in the PSF-subtracted frames constructed in the way described above.

To calibrate the transmission of the coronagraph, a standard star (HD 1274) was taken during the programme 384.C-0245A, once outside and once below the coronagraph, and reduced in the same way as the exposures of the science targets. The flux values have been integrated within apertures of 19 pixels radius which fits well inside the coronagraph. Relating the measurements inside and outside the coronagraph gives a transmission of 0.47 ± 0.03 % in the K_s band which translates to a dimming of 5.83 ± 0.06 mag. The error bar accounts for uncertainties involved in the aperture photometry but not for other systematics like cross-talk, light-leaks, temporal variation of the PSF, improper/variable placement of the star below the coronagraph, or variable residual absorption by the transparent substrate which carries the coronagraphs. The new measurement gives a dimming weaker by half a magnitude than the value given in the NACO manual ($K_s = 6.3 \pm 0.1$ mag). The latter measurement was done in a way similar to the present work but using frames reduced in a different way and using peak counts instead of aperture photometry (ESO, priv. comm.). A conservative estimate of 6.1 ± 0.3 has been adopted in the present work since the discrepancy cannot be explained with the data available.

For each one of the companion candidates, the average magnitude of two epochs has been adopted and the uncertainty is given by half their difference plus the square-added error bar of 0.3 mag of the transmissivity of the coronagraph. For single-epoch images, the transmissivity is the only well-known dominant source of error.

4. Assessment of field coverage and detection limits

We could not take advantage of the full field of view of the NACO mode applied (28”x28”) since the corners are affected by obstructions. Furthermore, the coronagraphs themselves are insensitive patches in the field of view.

The field of view is covered completely between angular separations of 0.″35 (coronagraphic radius) and 9.″0 which correspond to different linear scales depending on the distance of the star. The parallaxes of the sample stars vary from 37 mas

(HIP 104383) to 311 mas (HD 22049) so that the field of view covers very different parts of the stellar environments, e.g. the closest view in the case of ϵ Eri (=HD 22049; 1.1 – 29 au) and the farthest view for HIP 104383 (9.2 – 237 AU) (Table B.1). The expected widest bound orbit of low-mass companions has been estimated based on the linear law given in Close et al. 2003 given the central mass of the target systems.

Although the field of view is complete only up to separations of ∼9", it samples separations of up to ∼25" corresponding to as much as ∼650 au in the case of HD 125451 and HIP 104383. Still the field of view never reaches the widest possible bound orbit in the present sample. We note, however, that inclination is a free parameter in this whole consideration and that measured separations are projected separations. Stars with exoplanets are known for which very wide (up to one third of a parsec) companions with common proper motion have been detected (Mugrauer et al. 2014).

To understand the detection limits in the wings of the PSF, we built noise maps from the reduced and PSF-subtracted images. We measured the standard deviation at each pixel using 7x7 adjacent pixels. This value has been multiplied by the square root of the number of pixels in an aperture of 13 pixels across in order to compare to the photometric flux measurements described above.

Based on the noise analysis, the limiting magnitudes have been derived relative to the magnitude of the primary star in the same way as by Brandeker et al. (2006). We found that a source can be detected at a given location if the flux measured is larger than a detection limit of $5 - 10\,\sigma$ of the local noise level and adopted the conservative and common value of 10σ. The limits derived have been corrected for the coronagraphic attenuation of 6.1mag inferred above. For each exposure, the right panel of Fig. 2 shows the average value of pixels at same angular distance.

When it comes to the determination of the mass of a companion that is still detectable, uncertain age is the largest contribution to the error budget. Using the stellar K_s band magnitude and the measured dynamic range, we calculated the K_s band magnitude of faint objects which could still have been detected at a given separation. The magnitudes have been interpolated in evolutionary models to obtain a mass estimate. We used the COND03 models (Baraffe et al. 2003) for effective temperatures lower than 1,300 K[8] and DUSTY00 (Chabrier et al. 2000) models for temperatures higher than 1,300 K. For ages of 100 Myr, 500 Myr, and 1 Gyr, this temperature corresponds to a mass of 10, 31, and 42 $M_{\rm Jup}$, respectively, and is accessible to the present survey. In this range of mass, the difference in K band magnitude between 100 Myr and 1 Gyr varies from 4 at the high-mass end to 8 at the low-mass end. Even if we avoid interpolating the true age range of the UMa group in the evolutionary models, we can assess that the age uncertainty of the UMa group implies an error of several K band magnitudes which is the dominant source of error in the present study.

5. Results and Discussion

The noise level is observed to decrease strongly with increasing separation from the primary star (Fig. 2). The longest on-target exposure time was spent on the brightest target, HD 22049, resulting in the highest dynamic range of the present work

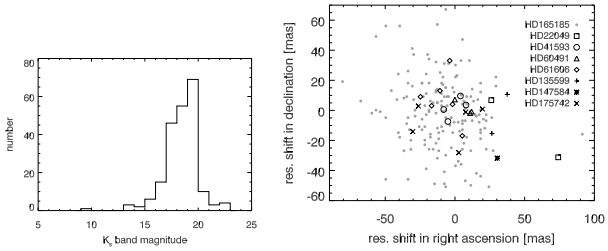

Fig. 3. Left: K_s magnitude distribution of candidates. Based on Table D.2. Errors in magnitude have not been considered. Right: residual motion of candidates. For all candidates detected in two epochs, the figure shows the residual shifts in right ascension and declination over the time elapsed between the epochs (Table D.2) after correcting for the proper and parallactic motion of the central stars (Table E.2). The symbols discern the candidates according to their central stars. Error bars have been omitted for clarity.

(≳17 mag for a $10\,\sigma$ detection). Typically, the dynamic range for a $10\,\sigma$ detection limit ranges between $\Delta K_s = 13$ and 15 at a separation beyond 3" (Figs. 1, E.1, E.2, and E.3). Given the K band magnitude of the central star, this corresponds to about $12-20\,M_{\rm Jup}$ provided an age of 500 Myr (Figs. E.4 and E.5). Objects with $12\,M_{\rm Jup}$ and younger than 1 Gyr could have been detected at separations of less than 10 au in the case of HIP 57548 with the deepest exposure of the present work, and objects with $20\,M_{\rm Jup}$ closer than 3 au (Table E.1).

More than 200 candidates have been identified (Figs. C.1-C.5, Table D.2). While in some fields, not a single object has been detected around the star (HD 11171, HD 26923, HD 38393, HD 63433, HIP 57548, HD 95650, HD 125451, HD 139006, and HD 217813), some 160 have been found around HD 165185 which is located in the galactic plane. A number of additional candidates have been found close to HD 11131, HD 22049, HD 26913, HD 41593, HD 60491, HD 61606 A, HD 135599, HD 147584, HD 175742, and HIP 104383 A[9].

The relative shift of a companion w.r.t. the star has been measured when a second epoch was available (Table D.2). All those cases are non-moving background stars when comparing to the predicted shift due to the stellar parallactic and proper motion (Table E.2 and Fig. 3)[10]. The deviation from these expectations is less than 0.″1 in all cases and of the order of the astrometric error bars (Table D.2). This shows that the true astrometric uncertainties agree with the assessments by Chauvin et al. (2010) implemented here (Sect. 3).

The detection limits can be compared to the brightness of faint background objects detected in the field of view. The uncertainties of the photometric measurements are below 1 mag in almost all cases. Usually, they are close to 0.5 mag and increasing towards the detection limit while the photometric measurements deviate by less than a magnitude from epoch to epoch. Enhanced error bars can be ascribed to smearing, noise, flux missed by the

[8] According to Baraffe et al. (2003), the COND03 models are more appropriate below 1300 K to predict infrared colours, for methane dwarfs and extrasolar giant planets at large orbital separation. The difference between the K_s and the K band has been neglected in the present study.

[9] HIP 104383 A is a special case since it appears as a visual binary below the coronagraph (Fig. D.1). According to Balega et al. (2004), it is a binary with a separation of 0.″3 and a magnitude difference of 1.67 in the R' band. In the K_s band we measured a magnitude difference of 0.45. The astrometric measurements presented here have been done w.r.t. the brighter component while the co-added signal has been used for photometric measurements.

[10] The parallactic motion has been calculated assuming a value of the obliquity of the ecliptic plane of 23.°4 and expressing the solar longitude by $L = 279.^\circ 697 + 36,000.^\circ 770\,T$ with the time T given by Julian centuries since 1900, January 0, 12 h (Kovalevsky 1995). The eccentricity of Earth's orbit has been neglected.

Table 1. Identification of candidates with previous detections.

target/cand.	epoch/position		reference/magnitude/ID	
HD 22049	2002-08-20		(1)	
ID0001	4.″5	17.″0	K' = 17.3	2
ID0002	−9.″6	14.″2	K' = 17.3	1
HD 41593	2002-2004		(2)	
ID0002	11.″10	328.°40	H = 15.88	cc1
HD 175742	2004-06-28		(3)	
ID0001	9.″45	308.°5	K_s = 16.99 ± 0.09	3
ID0003	7.″57	335.°5	K_s = 19.13 ± 0.23	4
ID0004	2.″64	89°	K_s = 16.88 ± 0.09	1
ID0006	9.″36	199°	K_s = 17.34 ± 0.09	2
HD 175742	2011-05-23		(4)	
ID0004	1.″72	1.″97	...	...

Notes. For each target with previous imaging, the candidates recovered are listed and the corresponding previous astrometric and photometric measurements are given together with the reference ID assigned in the previous work. Relative positions in right ascension and declination are given for Macintosh et al. (2003) (1) and Janson et al. (2013) (4) while total separation and position angle are given for Itoh et al. (2008b) (2) and Metchev & Hillenbrand (2009) (3).

aperture photometry at the edges of the frame, or background features like diffraction spikes, ghosts, and reflections (indicated in Table D.2).

The faintest object identified (HD 165185, ID0101) advocates an empirical detection limit of $K_s \approx 22$ for HD 165185. However, the aperture photometry of this object is affected by insufficient background correction so that it must be somewhat brighter (Fig. C.3). Moreover, the lower envelope to the distribution of most candidates (Fig. E.2) is a bit higher as is also indicated by the brightness distribution of all candidates (cf. Fig. 3). It covers magnitudes in the range $K_s = 13 - 23$ with a single brighter object next to HD 11131. As can be expected for a distribution of field stars, there are a few bright objects and a larger number of faint objects. The number of objects decreases rapidly at a brightness level fainter than $K_s = 20$ indicating that the census is complete down to this value. Since the distribution is almost entirely constituted of objects next to HD 165185, this completeness limit is certainly valid for this subset.

We compared our candidates with previous work for targets in common with other surveys which have not necessarily been dedicated to the UMa group (Macintosh et al. 2003; Itoh et al. 2008b; Metchev & Hillenbrand 2009).We recovered all of the previously known candidates (Table 1) at the positions expected as far as they are covered by our field of view. Photometric measurements agree well within the error bars as long as they have been measured in the same or a similar photometric band. The single exception is ID 4 next to HD 175742 (Metchev & Hillenbrand 2009, object 1). Most certainly, the difference of one K_s magnitude can be explained by the location of ID 4 in the PSF of HD 175742 where the photometric measurement is very sensitive to imperfections of the PSF subtraction. The same object was found by Janson et al. (2013) but no photometric measurement is given there. The southern component of HD 165185 listed by Mason et al. (2014) is out of the field of view of the present work but displayed in Table B.1.

The deepest exposure has been chosen for each target to derive a survey upper limit on the frequency of stars with a companion of given mass and age. This has been done in a basic way similar to Lafrenière et al. (2007) without assuming any prior knowledge on the mass-period distribution of companions.

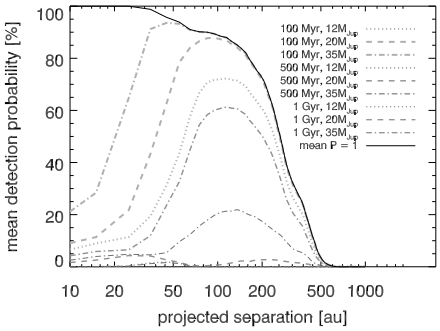

Fig. 4. Mean survey detection probability for companions of 12, 20, and 35 M_{Jup} as a function of separation and for different age of 100 Myr, 500 Myr, and 1 Gyr as indicated in the legend. The solid line gives the limiting case of a detection probability of 1 in each frame.

For this purpose, maps of $10\,\sigma$ detection probability have been derived from the maps of limiting magnitude presented in Sect. 4 by comparing them to the signal of a 12, 20, and 35 M_{Jup} companion at different ages of 100 Myr, 500 Myr, and 1 Gyr (using the evolutionary models described in Sect. 4)[11]. The mean survey detection probability has been assessed by centering, rescaling, and averaging those probability maps (Fig. 4). In the limiting case, where the detection probability equals 1 throughout each frame, the average detection probability is only limited by the respective field of view and approaches zero at separations beyond ∼500 au which are not covered by any exposure of the survey. The age range considered has a stronger effect than the mass range. On average, the survey is most sensitive at separations between 100 and 200 au since the distance of the targets and thus the field of view covered is very different.

We derived the upper limit on the frequency of stars with a companion where the mean $10\,\sigma$ detection probability is high. We followed the Bayesian approach described by Lafrenière et al. (2007) using the Poisson approximation and a confidence level of 95 %. In the most sensitive range between 100 and 200 au, we can place an upper limit of ∼25 % on the frequency of UMa group members with low-mass companions more massive than 35 M_{Jup} if the age of the UMa group is close to 500 Myr or younger. The limit is never below 15 %, defined by the number of stars, the confidence level, and the case of a detection probability of one everywhere (solid line in Fig. 4).

When interpreting the outcome of the present study one has to be aware of specific formation environments represented by the significant fraction of targets with stellar companions (cf. Tables A.2 and B.1). In addition we note that the known companions of GJ 569 have not been considered for the frequency estimate since they are closer to the star than the field covered by the present work and we did not account for the companions of HD 130948 since they have masses close to the Deuterium burning limit of $12 - 13\,M_{Jup}$ which we are not sensitive to on average. Although the results are not at variance with previous work, it is obvious that the study of the UMa group would benefit from a larger sample size. So far, northern UMa group members have not been studied systematically. Those actually comprise the largest part of the UMa group. Although its densest part on the northern hemisphere is within 30 pc, the group extends far beyond.

[11] The probability has been computed that a signal exceeds the $10\,\sigma$ detection threshold in the presence of noise, assuming a normal distribution.

Acknowledgements. M.A. thanks Eike W. Guenther for fruitful discussions. We thank the anonymous referee for the constructive comments. AB acknowledges support from DFG in grants NE 515/13-1 and 13-2. M.A. was supported by a graduate scholarship of the Cusanuswerk, one of the national student elite programs of Germany, and an individual fellowship granted by the Fundação para a Ciência e a Tecnologia (FCT), Portugal (reference SFRH/BPD/26817/2006). M.A. acknowledges research funding granted by the Deutsche Forschungsgemeinschaft (DFG) under the project RE 1664/4-1. M.A. further acknowledges support by DLR under the projects 50OW0204 and 50OO1501. RN acknowledges general support from the German National Science Foundation (Deutsche Forschungsgemeinschaft, DFG) in grants NE 515/13-1, 13-2, and 23-1. TOBS would like to thank Evangelisches Studienwerk e. V. Villigst, the state of Thuringia as well as DFG for support in program NE 515/30-1. RN and RE would like to thank DFG for support in the Priority Programme SPP 1385 on the *First ten Million years of the Solar System* in project NE 515 / 34-1 and 34-2. Use was made of the CDS services SIMBAD, Vizier, and the NASA/ADS abstract service. This research has made use of the Washington Double Star Catalog maintained at the U.S. Naval Observatory. This publication makes use of data products from the Two Micron All Sky Survey, which is a joint project of the University of Massachusetts and the Infrared Processing and Analysis Center/California Institute of Technology, funded by the National Aeronautics and Space Administration and the National Science Foundation.

References

Alibert, Y., Mordasini, C., Benz, W., & Winisdoerffer, C. 2005, A&A, 434, 343
Allende Prieto, C. & Lambert, D. L. 1999, A&A, 352, 555
Ammler, M. 2006, PhD thesis, Astrophysikalisches Institut und Universitätsternwarte Jena, Schillergäßchen 2-3, 07743 Jena, Germany
Ammler-von Eiff, M., Bedalov, A., Mugrauer, M., Neuhäuser, R., & Guenther, E. 2009, in AIP Conf. Proc., Vol. 1094, COOL STARS, STELLAR SYSTEMS AND THE SUN: Proceedings of the 15th Cambridge Workshop on Cool Stars, Stellar Systems and the Sun, St. Andrews (Scotland), 21-25 July 2008, 828
Ammler-von Eiff, M. & Guenther, E. W. 2009, A&A, 508, 677
Balega, I., Balega, Y. Y., Maksimov, A. F., et al. 2004, A&A, 422, 627
Bannister, N. P. & Jameson, R. F. 2007, MNRAS, 378, L24
Banse, K., Crane, P., Ounnas, C., & Ponz, D. 1983, in Proc. of DECUS, Zurich, 87
Baraffe, I., Chabrier, G., Barman, T. S., Allard, F., & Hauschildt, P. H. 2003, A&A, 402, 701
Benedict, G. F., McArthur, B. E., Gatewood, G., et al. 2006, AJ, 132, 2206
Biller, B. A., Liu, M. C., Wahhaj, Z., et al. 2010, ApJ, 720, L82
Biller, B. A., Liu, M. C., Wahhaj, Z., et al. 2013, ApJ, 777, 160
Boccaletti, A., Lagrange, A.-M., Bonnefoy, M., Galicher, R., & Chauvin, G. 2013, A&A, 551, L14
Bonavita, M. & Desidera, S. 2007, A&A, 468, 721
Bouvier, J., Kendall, T., Meeus, G., et al. 2008, A&A, 481, 661
Bowler, B. P., Liu, M. C., Shkolnik, E. L., & Tamura, M. 2015, ApJS, 216, 7
Brandeker, A., Jayawardhana, R., Khavari, P., Haisch, Jr., K. E., & Mardones, D. 2006, ApJ, 652, 1572
Brandt, T. D. & Huang, C. X. 2015, ArXiv e-prints
Broeg, C. 2007, MNRAS, 377, L44
Bulut, I. & Demircan, O. 2007, MNRAS, 378, 179
Burrows, A., Marley, M., Hubbard, W. B., et al. 1997, ApJ, 491, 856
Chabrier, G., Baraffe, I., Allard, F., & Hauschildt, P. 2000, ApJ, 542, 464
Chauvin, G., Lagrange, A.-M., Bonavita, M., et al. 2010, A&A, 509, A52
Chauvin, G., Lagrange, A.-M., Zuckerman, B., et al. 2005, A&A, 438, L29
Close, L. M., Siegler, N., Freed, M., & Biller, B. 2003, ApJ, 587, 407
Cushing, M. C., Kirkpatrick, J. D., Gelino, C. R., et al. 2011, ApJ, 743, 50
Deller, A. T. & Maddison, S. T. 2005, ApJ, 625, 398
Devillard, N. 1997, The Messenger, 87, 19
Devillard, N. 2011, in Astrophysics Source Code Library, record ascl:1112.001, 12001
Duchêne, G., Bontemps, S., Bouvier, J., et al. 2007, A&A, 476, 229
Eggen, O. J. 1994, in Galactic and Solar System Optical Astrometry, 191–+
Eggen, O. J. 1995, AJ, 110, 2862
Eggleton, P. P. & Tokovinin, A. A. 2008, MNRAS, 389, 869
Eisenbeiss, T., Ammler-von Eiff, M., Roell, T., et al. 2013, A&A, 556, A53
Eisenbeiss, T., Seifahrt, A., Mugrauer, M., et al. 2007, Astronomische Nachrichten, 328, 521
Fabricius, C., Høg, E., Makarov, V. V., et al. 2002, A&A, 384, 180
Fischer, D. A., Howard, A. W., Laughlin, G. P., et al. 2014, Protostars and Planets VI, 715
Fuhrmann, K. 2004, Astronomische Nachrichten, 325, 3
Gray, D. 2005, The observation and analysis of stellar photospheres, 3rd edn. (Cambridge: Cambridge University Press)
Guenther, E. W., Paulson, D. B., Cochran, W. D., et al. 2005, A&A, 442, 1031
Hatzes, A. P., Cochran, W. D., McArthur, B., et al. 2000, ApJ, 544, L145
Ida, S. & Lin, D. N. C. 2004, ApJ, 604, 388
Itoh, Y., Hayashi, M., Tamura, M., et al. 2008a, PASJ, 60, 223
Itoh, Y., Oasa, Y., & Fukagawa, M. 2006, ApJ, 652, 1729
Itoh, Y., Tamura, M., Hayashi, M., et al. 2008b, PASJ, 60, 209
Janson, M., Brandner, W., Henning, T., et al. 2007, AJ, 133, 2442
Janson, M., Brandt, T. D., Moro-Martín, A., et al. 2013, ApJ, 773, 73
King, J. R. & Schuler, S. C. 2005, PASP, 117, 911
King, J. R., Villarreal, A. R., Soderblom, D. R., Gulliver, A. F., & Adelman, S. J. 2003, AJ, 125, 1980
Kirkpatrick, J. D. 2008, in Astronomical Society of the Pacific Conference Series, Vol. 384, 14th Cambridge Workshop on Cool Stars, Stellar Systems, and the Sun, ed. S. P. P. S. D. E. M. B. J. Messina, 85–+
König, B., Fuhrmann, K., Neuhäuser, R., Charbonneau, D., & Jayawardhana, R. 2002, A&A, 394, L43
Kovalevsky, J. 1995, Modern Astrometry (Springer)
Lafrenière, D., Doyon, R., Marois, C., et al. 2007, ApJ, 670, 1367
Lenzen, R., Hartung, M., Brandner, W., et al. 2003, in Presented at the Society of Photo-Optical Instrumentation Engineers (SPIE) Conference, Vol. 4841, Instrument Design and Performance for Optical/Infrared Ground-based Telescopes. Edited by Iye, Masanori; Moorwood, Alan F. M. Proceedings of the SPIE, Volume 4841, pp. 944-952 (2003)., ed. M. Iye & A. F. M. Moorwood, 944–952
Lodieu, N., Boudreault, S., & Béjar, V. J. S. 2014, MNRAS, 445, 3908
Macintosh, B. A., Becklin, E. E., Kaisler, D., Konopacky, Q., & Zuckerman, B. 2003, ApJ, 594, 538
Malkov, O., Piskunov, A., & Zinnecker, H. 1998, A&A, 338, 452
Marengo, M., Megeath, S. T., Fazio, G. G., et al. 2006, ApJ, 647, 1437
Martín, E. L., Koresko, C. D., Kulkarni, S. R., Lane, B. F., & Wizinowich, P. L. 2000, ApJ, 529, L37
Mason, B. D., Wycoff, G. L., Hartkopf, W. I., Douglass, G. G., & Worley, C. E. 2001, AJ, 122, 3466
Mason, B. D., Wycoff, G. L., Hartkopf, W. I., Douglass, G. G., & Worley, C. E. 2014, VizieR Online Data Catalog, 1, 2026
McCarthy, C. & Zuckerman, B. 2004, AJ, 127, 2871
Metchev, S. A. & Hillenbrand, L. A. 2009, ApJS, 181, 62
Montes, D., López-Santiago, J., Gálvez, M. C., et al. 2001, MNRAS, 328, 45
Mugrauer, M., Ginski, C., & Seeliger, M. 2014, MNRAS, 439, 1063
Neuhäuser, R. & Guenther, E. W. 2004, A&A, 420, 647
Neuhäuser, R., Guenther, E. W., Alves, J., et al. 2003, Astronomische Nachrichten, 324, 535
Neuhäuser, R., Mugrauer, M., Fukagawa, M., Torres, G., & Schmidt, T. 2007, A&A, 462, 777
Neuhäuser, R. & Schmidt, T. 2012, in Topics in Adaptive Optics, ed. R. K. Tyson (Rijeka, Croatia: InTech)
Perryman, M. A. C., Lindegren, L., Kovalevsky, J., et al. 1997, A&A, 323, L49
Persson, S. E., Murphy, D. C., Krzeminski, W., Roth, M., & Rieke, M. J. 1998, AJ, 116, 2475
Potter, D., Martín, E. L., Cushing, M. C., et al. 2002, ApJ, 567, L133
Quillen, A. C. & Thorndike, S. 2002, ApJ, 578, L149
Rameau, J., Chauvin, G., Lagrange, A.-M., et al. 2013, A&A, 553, A60
Rousset, G., Lacombe, F., Puget, P., et al. 2003, in Presented at the Society of Photo-Optical Instrumentation Engineers (SPIE) Conference, Vol. 4839, Adaptive Optical System Technologies II. Edited by Wizinowich, Peter L.; Bonaccini, Domenico. Proceedings of the SPIE, Volume 4839, pp. 140-149 (2003)., ed. P. L. Wizinowich & D. Bonaccini, 140–149
Simon, M., Bender, C., & Prato, L. 2006, ApJ, 644, 1183
Skrutskie, M. F., Cutri, R. M., Stiening, R., et al. 2006, AJ, 131, 1163
Skuljan, J., Ramm, D. J., & Hearnshaw, J. B. 2004, MNRAS, 352, 975
Tokovinin, A., Thomas, S., Sterzik, M., & Udry, S. 2006, A&A, 450, 681
Tokunaga, A. T., Simons, D. A., & Vacca, W. D. 2002, PASP, 114, 180
Valenti, J. A. & Fischer, D. A. 2005, ApJS, 159, 141
van Leeuwen, F. 2007, A&A, 474, 653
Wahhaj, Z., Liu, M. C., Biller, B. A., et al. 2011, ApJ, 729, 139
Warmels, R. H. 1992, in Astronomical Society of the Pacific Conference Series, Vol. 25, Astronomical Data Analysis Software and Systems I, ed. D. M. Worrall, C. Biemesderfer, & J. Barnes, 115
Yamamoto, K., Matsuo, T., Shibai, H., et al. 2013, PASJ, 65, 90
Zapatero Osorio, M. R., Lane, B. F., Pavlenko, Y., et al. 2004, ApJ, 615, 958
Zechmeister, M., Kürster, M., Endl, M., et al. 2013, A&A, 552, A78

Appendix A: Sample

Appendix B: Field of view and nearby visual companions

Appendix C: Images with candidates

Appendix D: List of candidates

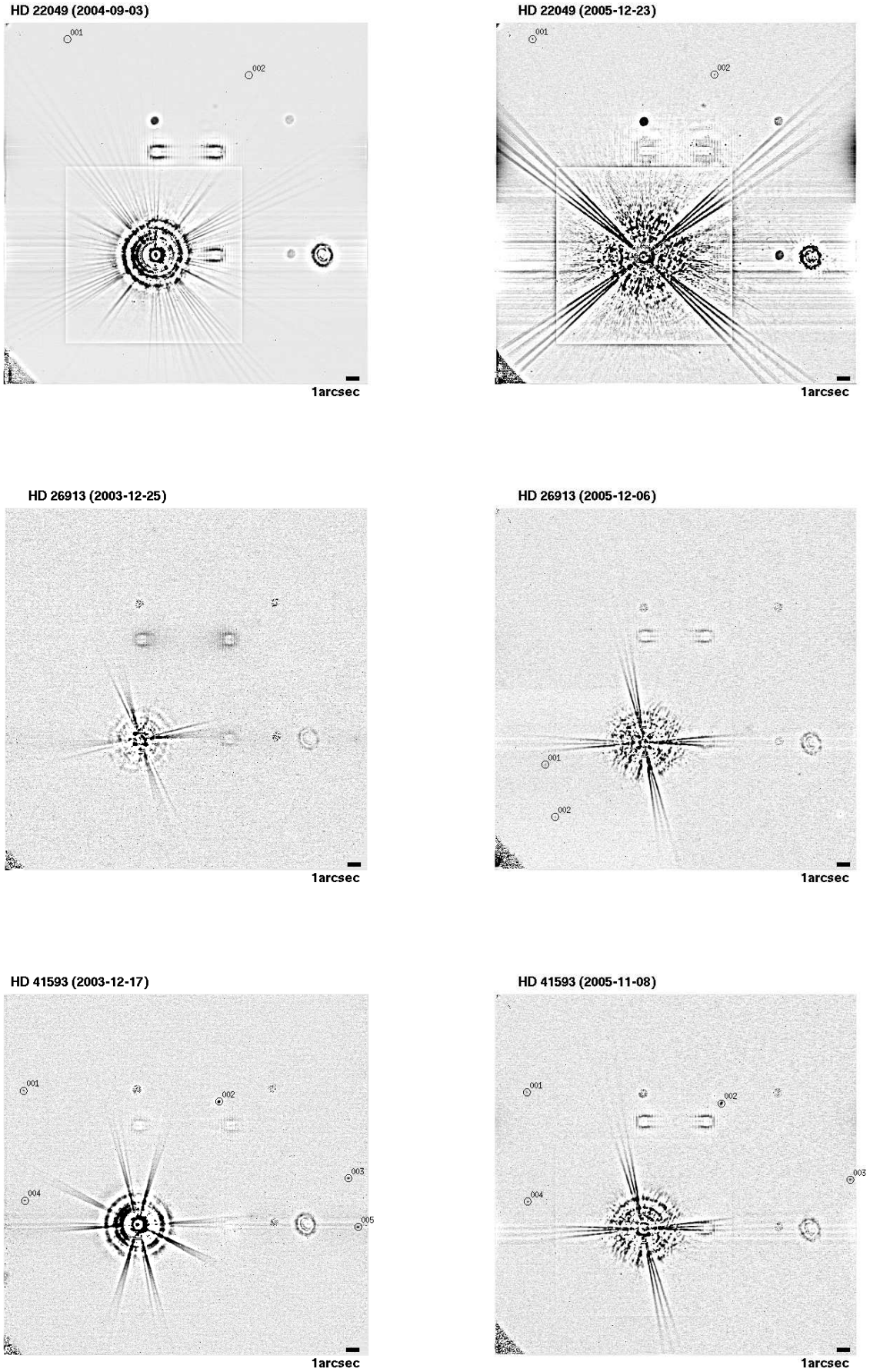

Fig. C.1. Candidates for stars with images in two epochs: HD 22049, HD 26913, and HD 41593. The images display the central star under the coronagraph. Faint companion candidates in the field of view are indicated by circles and are enumerated (cf. Table. D.2). The scale is indicated in the image. North is at the top and East is to the left. The PSF of the central star has been removed in a rectangular area centred on the star and a smoothed image has been subtracted. The residual speckle pattern and the diffraction spikes of the mount of the secondary mirror remain visible (several of those due to the addition of several exposures). In addition, there are reflections, ghosts, a vignetted region to the lower left, and the shadows of the other three coronagraphs.

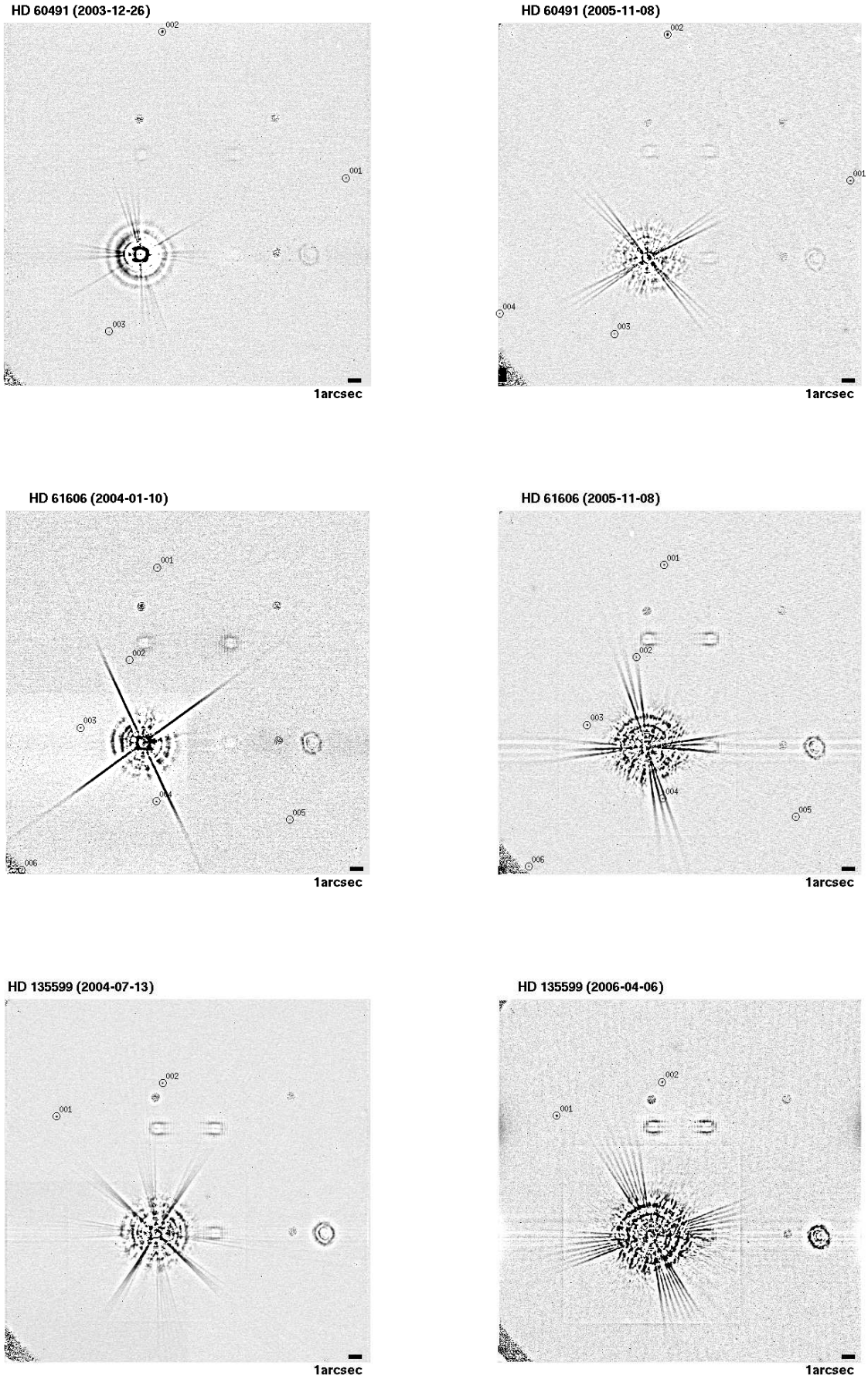

Fig. C.2. Candidates for stars with images in two epochs: HD 60491, HD 61606, and HD 135599. The layout is the same as in Fig. C.1.

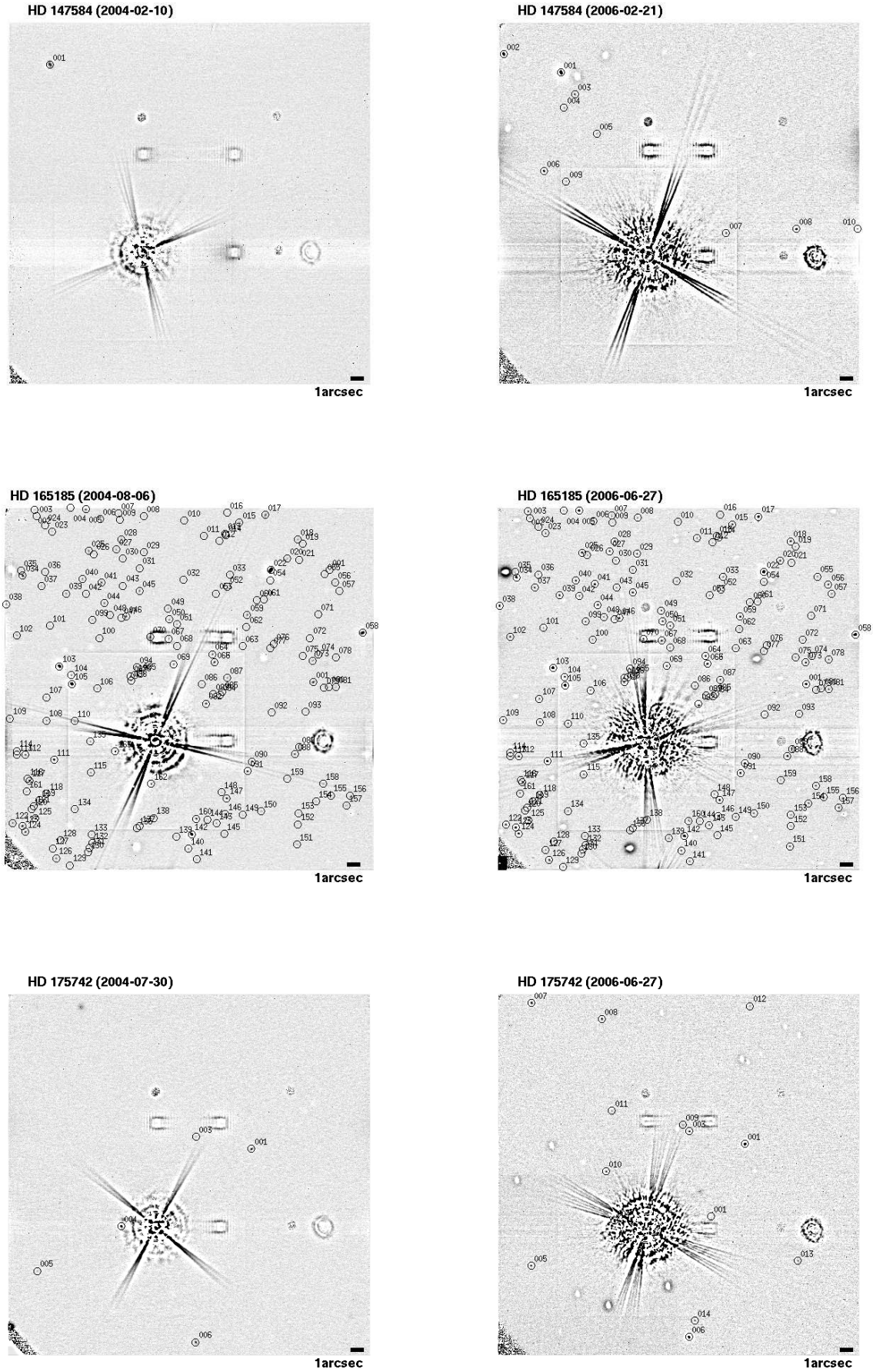

Fig. C.3. Candidates for stars with images in two epochs: HD 147584, HD 165185, and HD 175742. The layout is the same as in Fig. C.1. Stellar residuals are present in the second epochs since jittering of the sky exposures did not work in those cases.

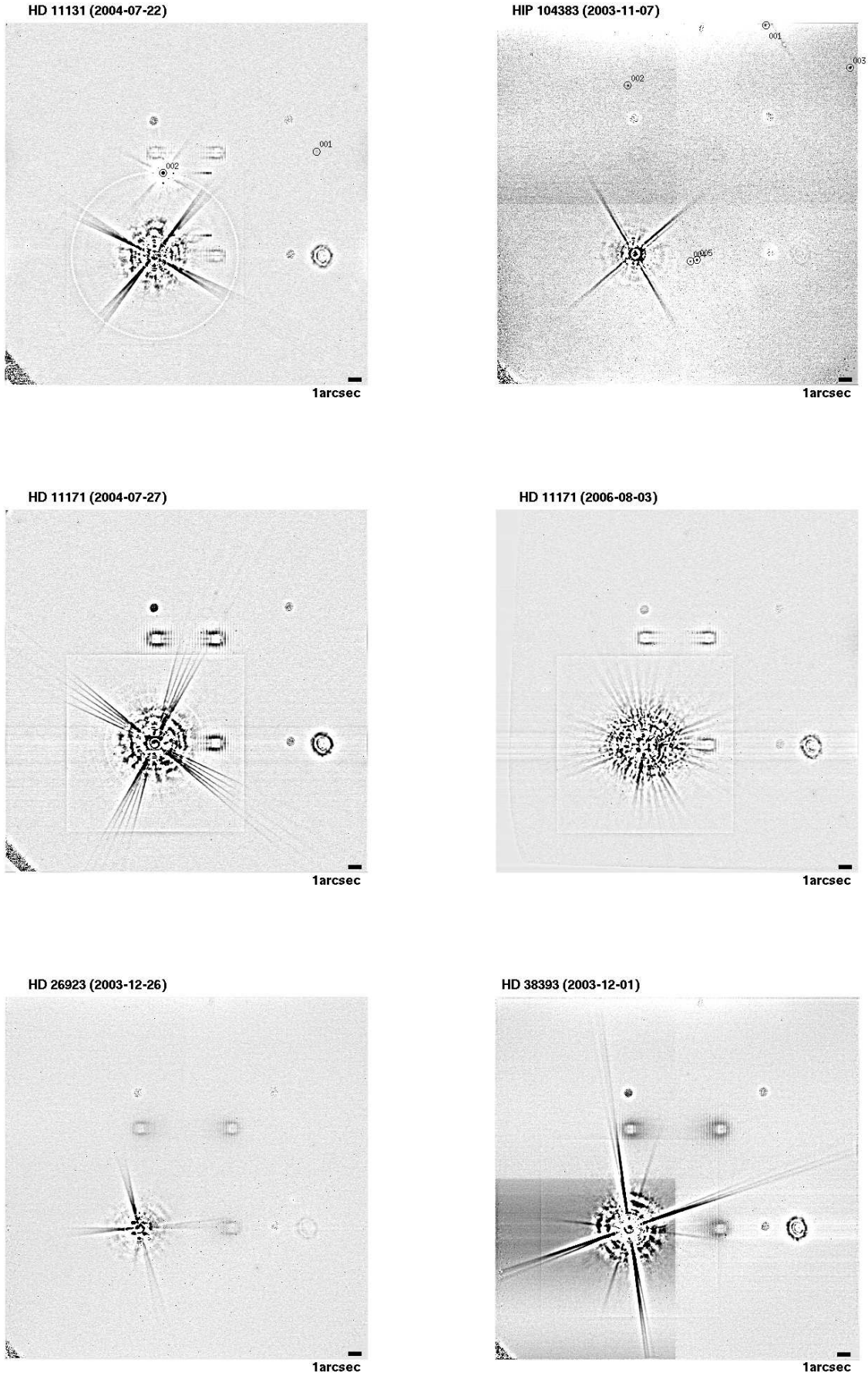

Fig. C.4. Candidates found in single-epoch observations (HD 11131 and HIP 104383) and observations of stars without any candidates (HD 11171, HD 26923, HD 38393). The layout is the same as in Fig. C.1. HIP 104383 A is a double star below the coronagraph (see Fig. D.1 and footnote to Sect. 5).

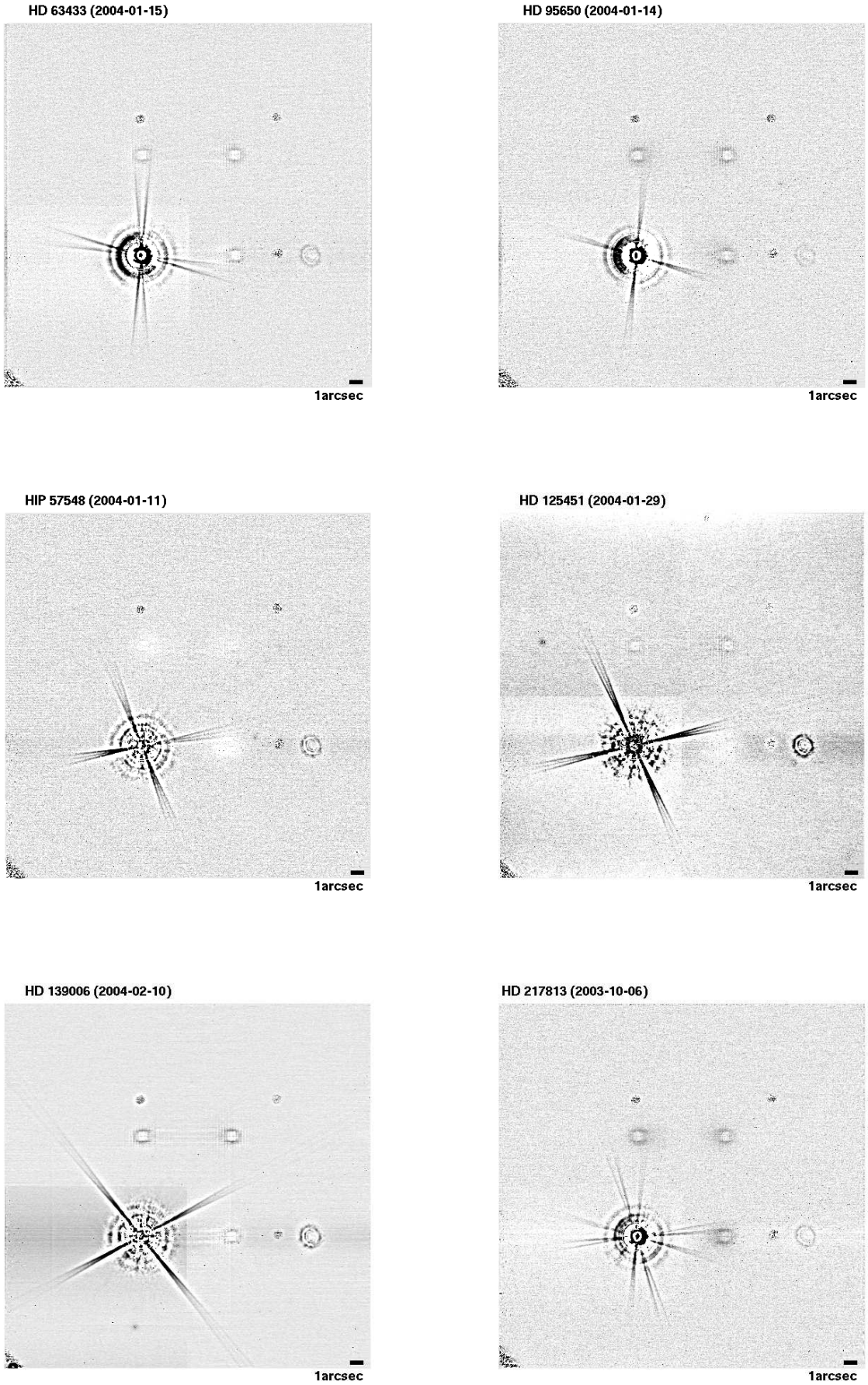

Fig. C.5. Observations of stars without any candidates: HD 63433, HD 95650, HIP 57548, HD 125451, HD 139006, and HD 217813. The layout is the same as in Fig. C.1.

Table A.1. The sample of UMa group members.

name	Montes et al. (2001)		King et al. (2003)			Fuhrmann (2004)	proper motion [mas/yr]		number of
	V_{pec}	ρ_C	kin.	phot.	final		$\mu_\alpha \cos\delta$	μ_δ	NACO epochs
HD 11131	Y	Y	?	Y?	Y?	Y	-124.54 ± 3.03	-105.82 ± 2.93	1
HD 11171	Y	Y	?/Y?	Y?	Y?	Y	-148.11 ± 0.25	-93.43 ± 0.24	2
HD 22049	...	...	...	...	...	Y	-975.17 ± 0.21	19.49 ± 0.20	2
HD 26913	N	Y	?	?	?	Y	-102.64 ± 0.66	-113.30 ± 0.59	2
HD 26923	Y	Y	Y?	Y	Y?	Y	-109.46 ± 0.48	-108.25 ± 0.43	1
HD 38393	Y	Y	?/Y?	Y?	Y?	...	-291.67 ± 0.14	-368.97 ± 0.15	1
HD 41593	Y	Y	N?/?	Y	N?/?	Y	-120.46 ± 0.71	-103.21 ± 0.43	2
HD 60491	N	Y	N?/?	Y?	N?/?	...	-81.17 ± 1.26	-42.66 ± 0.66	2
HD 61606	N	Y	N?	Y?	N?	...	69.90 ± 0.71	-278.33 ± 0.31	2
HD 63433	Y	N	Y?	?	?	Y	-8.31 ± 0.65	-10.48 ± 0.46	1
HD 95650	N	Y	Y	Y?	Y	...	142.30 ± 1.16	-51.69 ± 0.79	1
HIP 57548	N	Y	N?	N?	N?	...	605.26 ± 2.32	-1219.28 ± 1.97	1
HD 125451	N	Y	...	...	...	...	105.95 ± 0.23	-31.80 ± 0.21	1
HD 135599	...	...	?	Y	?	Y	178.35 ± 0.66	-137.52 ± 0.62	2
HD 139006	...	...	Y	Y	Y	Y	120.27 ± 0.19	-89.58 ± 0.20	2
HD 147584	...	...	Y	Y	Y	...	199.97 ± 0.25	110.97 ± 0.43	2
HD 165185	N	Y	Y	Y?	Y	...	105.05 ± 0.60	7.95 ± 0.32	2
HD 175742	...	...	N?	Y?	?	...	131.31 ± 0.49	-283.72 ± 0.63	2
HIP 104383	N	Y	...	...	...	...	-77.56 ± 2.42	-32.89 ± 0.87	2
HD 217813	N	Y	?	?	?	Y	-117.70 ± 0.59	-27.66 ± 0.49	1

Notes. UMa membership information, proper motion (van Leeuwen 2007), and number of epochs of NACO observations obtained for the present work. We reiterate the assignments by Montes et al. (2001) and King et al. (2003) concerning the match of Eggen's criteria or, respectively, the decision on kinematic, photometric, and final membership ('Y' = yes; 'N' = no). Uncertainty is expressed by '?' and we refer the reader to King et al. (2003) for more information. Some of the stars were not observed (zero NACO epochs taken) as is explained in the text and omitted here.

Table A.2. Basic stellar data of the sample of UMa group members.

object	HIP number	α (2000.0)	δ (2000.0)	parallax [mas]	spec. type	V mag.	Ks mag.
HD 11131	8486	01 49 23.36	-10 42 12.8	44.32 ± 3.02	G1V	6.727	5.149
HD 11171	8497	01 49 35.10	-10 41 11.1	43.13 ± 0.26	F3III	4.664	3.872
HD 22049	16537	03 32 55.84	-09 27 29.7	310.94 ± 0.16	K2V	3.730	1.776
HD 26913	19855	04 15 25.79	+06 11 58.7	47.49 ± 0.68	G5IV	6.960	5.271
HD 26923	19859	04 15 28.80	+06 11 12.7	46.88 ± 0.47	G0IV	6.314	4.903
HD 38393	27072	05 44 27.79	-22 26 54.2	112.02 ± 0.18	F7V	3.586	2.508
HD 41593	28954	06 06 40.48	+15 32 31.6	65.48 ± 0.67	K0V	6.762	4.822
HD 60491	36827	07 34 26.17	-06 53 48.0	40.73 ± 1.00	K2V	8.160	6.019
HD 61606	37349	07 39 59.33	-03 35 51.0	70.37 ± 0.64	K2V	7.200	4.885
HD 63433	38228	07 49 55.06	+27 21 47.5	45.45 ± 0.53	G5IV	6.930	5.258
HD 95650	53985	11 02 38.34	+21 58 01.7	84.95 ± 1.05	M0	9.690	5.688
HIP 57548	57548	11 47 44.40	+00 48 16.4	298.04 ± 2.30	M4V	11.080	5.654
HD 125451	69989	14 19 16.28	+13 00 15.5	38.32 ± 0.28	F5IV	5.400	4.394
HD 135599	74702	15 15 59.17	+00 47 46.9	63.11 ± 0.70	K0	7.000	4.958
HD 139006	76267	15 34 41.27	+26 42 52.9	43.46 ± 0.28	A0V+G5V[a]	2.210	2.206
HD 147584	80686	16 28 28.14	-70 05 03.8	82.53 ± 0.52	F9V+M4V[b]	4.910	3.661
HD 165185	88694	18 06 23.72	-36 01 11.2	56.97 ± 0.48	G5V	5.949	4.469
HD 175742	92919	18 55 53.22	+23 33 23.9	46.74 ± 0.85	K0V[c]	8.090	5.637
HIP 104383	104383	21 08 45.47	-04 25 36.9	36.92 ± 1.53	K6+M1[d]	9.430	6.398
HD 217813	113829	23 03 04.98	+20 55 06.9	40.46 ± 0.57	G5V	6.652	5.148

Notes. All parallaxes are *HIPPARCOS* parallaxes (van Leeuwen 2007). K_s band magnitudes were taken from 2MASS (Skrutskie et al. 2006) and are combined magnitudes for tight binaries. For spectroscopic binaries, the spectral type is displayed for both components.
References for spectral type. [(a)] Bulut & Demircan (2007) [(b)] HD 147584: mean value of M4 of the range given by Skuljan et al. (2004) (M1V-M7V) [(c)] HD 175742: SB1 (Tokovinin et al. 2006); literature not unanimous on the parameters (Eggleton & Tokovinin 2008) [(d)] HIP 104383: Balega et al. (2004) .

Table B.1. Characterisation of the NACO field of view according to Fig. 1.

name	FOV		max.	nearby stellar companions				central	ref.	expected approx.
	inner	outer	FOV	#1	#2	ref.	WDS entry	mass		widest bound
	[au]	[au]	[au]	[au]	[au]			[$M_\odot$]		orbit [au]
HD 11131	8.3	213	590	4340	...	1	01496-1041	1.00	6	5400
HD 11171	8.3	213	590	4340	...	1	01496-1041	1.52	3	8200
HD 22049	1.1	29	80	...	...	..	...	0.79	6	4300
HD 26913	7.3	188	522	1350	...	1	04155+0611	0.96	6	5200
HD 26923	7.4	191	530	1360	...	1	04155+0611	1.07	6	5800
HD 38393	3.1	81	224	852	1250	2	05445-2227	1.23	4	6600
HD 41593	5.4	139	386	...	...	..	...	0.89	6	4800
HD 60491	8.7	223	620	...	...	..	...	0.86	10	4600
HD 61606	5.0	128	355	822	...	1	07400-0336	1.43	5	7700
HD 63433	7.6	196	545	...	...	..	...	0.99	6	5400
HIP 57548	1.2	30	83	...	...	..	...	0.30	12	1600
HD 95650	4.1	105	292	...	...	..	...	0.50	12	2700
HD 125451	9.1	235	652	4280	...	2	14193+1300	1.40	3	7600
HD 135599	5.5	140	389	...	...	..	...	0.85	6	4600
HD 139006	8.0	206	573	...	...	..	...	3.50	11	18900
HD 147584	4.2	109	303	...	...	..	...	1.39	8	7500
HD 165185	6.1	156	434	214	...	2	18064-3601	1.10	12	5900
HD 175742	7.5	193	536	...	...	..	...	1.10	9	5900
HD 217813	8.5	218	607	...	...	..	...	1.05	6	5700
HIP 104383	9.2	237	659	7	554	2	21088-0426	1.10	12	5900

Notes. (2, 3) Range of separations which are completely covered around the coronograph (from inner radius, i.e. outer bound of the coronagraph of 0.″35 to the outer radius of 9″ shown in Fig. 1). – **(4)** maximum (incomplete) field of view (25″) – **(5-8)** separation of up to two known nearby visual companions, reference, and WDS catalogue entry. – **(9, 10)** Mass of the central star/binary and reference – **(11)** Separation of the approximate widest expected bound orbit of very low-mass companions according to the approximation by Close et al. (2003) for masses greater than 0.185 $M_\odot$. Very close (spectroscopic) components are not listed but accounted for in the central mass. Masses have been derived separately for the binary components of HIP 104383 (0.6 $M_\odot$ and 0.5 $M_\odot$, respectively) and then added up. HD 147584 is a spectroscopic binary with components of 1.12 $M_\odot$ and 0.09 – 0.45 $M_\odot$ (Skuljan et al. 2004, an average of 0.27 $M_\odot$ has been adopted for the secondary). HD 175742 is a single-lined spectroscopic binary with a primary mass of 0.75 $M_\odot$ and a minimum mass of the secondary of 0.35 $M_\odot$ (Tokovinin et al. 2006). The maximum expected orbital separation is thus a lower limit in this particular case.

References. (1) Fabricius et al. (2002); (2) Mason et al. (2001, 2014); (3) Allende Prieto & Lambert (1999); (4) Ammler-von Eiff & Guenther (2009); (5) Bonavita & Desidera (2007); (6) Fuhrmann (2004); (7) Simon et al. (2006); (8) Skuljan et al. (2004); (9) Tokovinin et al. (2006); (10) Valenti & Fischer (2005); (11) Bulut & Demircan (2007); (12) based on spectral type (Table A.2) and Gray (2005, table 1).

Table D.2. Astrometry and photometry of candidates for each target and each epoch of observation.

ID	$\Delta\alpha$["]			$\Delta\delta$["]			$\Delta\alpha$["]			$\Delta\delta$["]			K_s [mag]			$\delta\Delta\alpha$[mas]			$\delta\Delta\delta$[mas]		
HD 11131	2004-07-22																				
ID0001	-12.437	±	0.022	7.981	±	0.033	...			...			18.8	±	0.3	...			...		
ID0002	-0.680	±	0.017	6.335	±	0.004	...			...			9.5	±	0.3	...			...		
HD 22049	2004-09-03						2005-12-23														
ID0001	6.749	±	0.044	16.607	±	0.020	8.558	±	0.044	16.731	±	0.025	17.2	±	0.5	1809	±	62	124	±	32
ID0002	-7.215	±	0.036	13.812	±	0.021	-5.454	±	0.037	13.974	±	0.016	17.3	±	0.4	1761	±	52	162	±	26
HD 26913	2003-12-25						2005-12-06														
ID0001	...			...			7.626	±	0.006	-1.747	±	0.020	18.3	±	0.3	...			...		
ID0002	...			...			6.864	±	0.016	-5.755	±	0.018	18.6	±	0.3	...			...		
HD 41593	2003-12-17						2005-11-08														
ID0001	8.784	±	0.027	10.313	±	0.024	8.966	±	0.028	10.507	±	0.024	17.8	±	0.4	182	±	39	194	±	34
ID0002	-6.208	±	0.025	9.453	±	0.017	-6.023	±	0.026	9.639	±	0.017	15.4	±	0.4	185	±	36	186	±	24
ID0003	-16.149	±	0.013	3.558	±	0.042	-15.951	±	0.014	3.755	±	0.042	16.8	±	0.5	198	±	19	197	±	59
ID0004	8.700	±	0.007	1.857	±	0.023	8.894	±	0.008	2.060	±	0.023	17.6	±	0.4	194	±	11	203	±	33
ID0005	-16.878	±	0.010	-0.197	±	0.044	...			...			16.2	±	0.3	...			...		
HD 60491	2003-12-26						2005-11-08														
ID0001	-15.721	±	0.018	5.847	±	0.041	-15.582	±	0.018	5.918	±	0.041	17.4	±	0.3	139	±	25	71	±	58
ID0002	-1.695	±	0.045	17.052	±	0.011	-1.567	±	0.045	17.132	±	0.011	15.6	±	0.3	128	±	64	80	±	16
ID0003	2.382	±	0.015	-5.890	±	0.007	2.522	±	0.015	-5.818	±	0.007	18.5	±	0.3	140	±	21	72	±	10
ID0004	...			...			11.312	±	0.013	-4.255	±	0.030	18.5	±	0.3	...			...		
HD 61606	2004-01-10						2005-11-08														
ID0001	-1.114	±	0.035	13.389	±	0.008	-1.324	±	0.036	13.898	±	0.009	17.7	±	0.3	-210	±	50	509	±	12
ID0002	1.021	±	0.017	6.328	±	0.005	0.819	±	0.018	6.831	±	0.005	19.0	±	0.9[a]	-202	±	25	503	±	7
ID0003	4.780	±	0.004	1.135	±	0.013	4.584	±	0.005	1.648	±	0.012	16.9	±	0.3	-196	±	6	513	±	18
ID0004	-1.017	±	0.012	-4.491	±	0.004	-1.204	±	0.010	-3.987	±	0.004	17.8	±	0.9[a]	-187	±	16	504	±	6
ID0005	-11.218	±	0.017	-5.886	±	0.030	-11.398	±	0.016	-5.403	±	0.030	18.1	±	0.3	-180	±	23	483	±	42
ID0006	9.264	±	0.026	-9.712	±	0.025	9.075	±	0.025	-9.179	±	0.024	18.2	±	0.3	-189	±	36	533	±	35
HD 135599	2004-07-13						2006-04-06														
ID0001	7.610	±	0.024	8.923	±	0.021	7.238	±	0.024	9.163	±	0.020	17.1	±	0.3	-372	±	34	240	±	29
ID0002	-0.490	±	0.030	11.476	±	0.007	-0.851	±	0.031	11.742	±	0.007	17.9	±	0.3	-361	±	43	266	±	10
HD 147584	2004-02-10						2006-02-21														
ID0001	7.082	±	0.038	14.442	±	0.020	6.702	±	0.037	14.197	±	0.020	13.4	±	0.8[b]	-380	±	53	-245	±	28
ID0002	...			...			11.121	±	0.041	15.617	±	0.031	15.1	±	0.3	...			...		
ID0003	...			...			5.645	±	0.033	12.509	±	0.017	17.7	±	0.3	...			...		
ID0004	...			...			6.463	±	0.030	11.456	±	0.018	18.5	±	0.3	...			...		
ID0005	...			...			3.956	±	0.025	9.465	±	0.012	19.5	±	0.3	...			...		
ID0006	...			...			8.022	±	0.018	6.592	±	0.021	16.5	±	0.3	...			...		
ID0007	...			...			-6.014	±	0.006	1.809	±	0.016	17.7	±	0.3	...			...		
ID0008	...			...			-11.427	±	0.009	2.109	±	0.030	16.4	±	0.3	...			...		
ID0009	...			...			6.303	±	0.016	5.777	±	0.017	19.2	±	0.3	...			...		
ID0010	...			...			-16.132	±	0.011	2.120	±	0.042	21.4	±	0.3	...			...		
HD 165185	2004-08-06						2006-06-27														
ID0001	-12.109	±	0.014	4.500	±	0.032	-12.367	±	0.014	4.475	±	0.032	16.7	±	0.4	-258	±	20	-25	±	45
ID0002	9.264	±	0.047	17.735	±	0.027	9.035	±	0.047	17.770	±	0.026	18.6	±	0.6	-229	±	66	35	±	37
ID0003	9.114	±	0.045	17.253	±	0.026	8.881	±	0.045	17.264	±	0.025	19.8	±	0.9[c]	-233	±	64	11	±	36
ID0004	6.524	±	0.047	17.879	±	0.020	6.301	±	0.047	17.840	±	0.020	21.8	±	2.1[c]	-223	±	66	-39	±	28
ID0005	5.351	±	0.047	17.779	±	0.018	5.110	±	0.047	17.834	±	0.017	17.0	±	0.8[c]	-241	±	66	55	±	25
ID0006	4.259	±	0.045	17.036	±	0.015	4.019	±	0.045	17.027	±	0.015	19.9	±	0.4	-240	±	64	-9	±	21

Table D.2. continued.

ID	$\Delta\alpha$["]			$\Delta\delta$["]			$\Delta\alpha$["]			$\Delta\delta$["]			K_s [mag]			$\delta\Delta\alpha$[mas]			$\delta\Delta\delta$[mas]		
ID0007	2.842	±	0.046	17.473	±	0.013	2.595	±	0.046	17.429	±	0.012	19.5	±	0.6	-247	±	65	-44	±	18
ID0008	0.875	±	0.045	17.248	±	0.010	0.610	±	0.045	17.277	±	0.010	19.4	±	0.5	-265	±	64	29	±	14
ID0009	2.753	±	0.044	16.955	±	0.012	2.534	±	0.044	16.901	±	0.012	22.3	±	1.5[d]	-219	±	62	-54	±	17
ID0010	-2.224	±	0.044	16.927	±	0.012	-2.515	±	0.044	16.964	±	0.012	19.5	±	0.3	-291	±	62	37	±	17
ID0011	-3.699	±	0.041	15.713	±	0.013	-3.968	±	0.041	15.710	±	0.014	19.2	±	0.5	-269	±	58	-3	±	19
ID0012	-4.902	±	0.040	15.352	±	0.016	-5.177	±	0.040	15.364	±	0.016	20.7	±	0.8[d]	-275	±	57	12	±	23
ID0013	-5.338	±	0.042	15.915	±	0.017	-5.481	±	0.042	15.887	±	0.017	19.1	±	0.4	-143	±	59	-28	±	24
ID0014	-5.415	±	0.041	15.784	±	0.017	-5.673	±	0.041	15.790	±	0.018	18.5	±	0.6	-258	±	58	6	±	25
ID0015	-6.450	±	0.044	16.762	±	0.020	-6.697	±	0.044	16.764	±	0.020	18.1	±	0.4	-247	±	62	2	±	28
ID0016	-5.497	±	0.046	17.530	±	0.018	-5.785	±	0.046	17.517	±	0.018	21.9	±	1.9[d]	-288	±	65	-13	±	25
ID0017	-8.445	±	0.046	17.338	±	0.024	-8.713	±	0.046	17.352	±	0.025	16.9	±	0.5	-268	±	65	14	±	35
ID0018	-10.926	±	0.041	15.457	±	0.030	-11.194	±	0.041	15.463	±	0.031	17.8	±	0.5	-268	±	58	6	±	43
ID0019	-11.310	±	0.040	15.103	±	0.031	-11.551	±	0.040	15.040	±	0.031	19.9	±	0.7	-241	±	57	-63	±	44
ID0020	-10.113	±	0.037	13.975	±	0.028	-10.377	±	0.037	13.970	±	0.028	18.1	±	0.5	-264	±	52	-5	±	40
ID0021	-11.011	±	0.037	13.883	±	0.030	-11.253	±	0.037	13.822	±	0.031	20.0	±	0.3	-242	±	52	-61	±	43
ID0022	-8.846	±	0.035	13.106	±	0.024	-9.117	±	0.035	13.102	±	0.025	13.8	±	0.5	-271	±	49	-4	±	35
ID0023	7.949	±	0.042	16.054	±	0.023	7.695	±	0.042	16.079	±	0.022	18.9	±	0.5	-254	±	59	25	±	32
ID0024	8.492	±	0.044	16.573	±	0.024	8.262	±	0.044	16.594	±	0.024	20.5	±	0.7	-230	±	62	21	±	34
ID0025	5.126	±	0.038	14.583	±	0.016	4.881	±	0.038	14.596	±	0.015	17.5	±	0.5	-245	±	54	13	±	22
ID0026	4.724	±	0.038	14.350	±	0.015	4.477	±	0.038	14.395	±	0.015	19.7	±	0.5	-247	±	54	45	±	21
ID0027	3.015	±	0.038	14.689	±	0.012	2.762	±	0.039	14.711	±	0.011	18.1	±	0.4	-253	±	54	22	±	16
ID0028	2.606	±	0.040	15.448	±	0.011	2.364	±	0.041	15.467	±	0.011	17.6	±	0.5	-242	±	57	19	±	16
ID0029	0.896	±	0.038	14.477	±	0.009	0.648	±	0.038	14.497	±	0.009	18.5	±	0.3	-248	±	54	20	±	13
ID0030	2.528	±	0.037	14.003	±	0.011	2.284	±	0.037	14.002	±	0.010	19.5	±	0.5	-244	±	52	—	±	15
ID0031	1.235	±	0.035	13.261	±	0.009	0.991	±	0.035	13.267	±	0.008	19.4	±	0.5	-244	±	49	6	±	12
ID0032	-2.163	±	0.032	12.380	±	0.009	-2.420	±	0.032	12.377	±	0.010	19.6	±	0.4	-257	±	45	-3	±	13
ID0033	-5.715	±	0.034	12.750	±	0.017	-5.990	±	0.034	12.723	±	0.017	18.9	±	0.5	-275	±	48	-27	±	24
ID0034	10.187	±	0.034	12.688	±	0.028	9.948	±	0.034	12.707	±	0.027	16.5	±	0.5	-239	±	48	19	±	39
ID0035	10.304	±	0.035	13.084	±	0.028	10.039	±	0.035	13.088	±	0.027	19.1	±	0.3	-265	±	49	4	±	39
ID0036	8.481	±	0.034	12.975	±	0.024	8.265	±	0.034	12.919	±	0.023	19.5	±	0.3	-216	±	48	-56	±	33
ID0037	8.773	±	0.032	11.895	±	0.024	8.539	±	0.032	11.913	±	0.023	18.5	±	0.5	-234	±	45	18	±	33
ID0038	11.459	±	0.028	10.500	±	0.031	11.254	±	0.028	10.510	±	0.030	17.4	±	0.5	-205	±	40	10	±	43
ID0039	6.865	±	0.030	11.321	±	0.019	6.626	±	0.030	11.318	±	0.019	17.9	±	0.4	-239	±	42	-3	±	27
ID0040	5.618	±	0.033	12.429	±	0.016	5.363	±	0.033	12.441	±	0.016	17.9	±	0.4	-255	±	47	12	±	23
ID0041	4.147	±	0.032	12.160	±	0.013	3.906	±	0.032	12.163	±	0.013	17.2	±	0.4	-241	±	45	3	±	18
ID0042	5.329	±	0.030	11.286	±	0.016	5.088	±	0.030	11.269	±	0.015	19.1	±	0.5	-241	±	42	-17	±	22
ID0043	2.489	±	0.031	11.910	±	0.010	2.237	±	0.031	11.904	±	0.009	19.4	±	0.6	-252	±	44	-6	±	13
ID0044	3.924	±	0.028	10.574	±	0.012	3.676	±	0.028	10.575	±	0.011	17.6	±	0.4	-248	±	40	1	±	16
ID0045	1.229	±	0.030	11.519	±	0.008	0.976	±	0.030	11.525	±	0.007	17.6	±	0.4	-253	±	42	6	±	11
ID0046	2.264	±	0.025	9.561	±	0.008	2.020	±	0.025	9.555	±	0.008	17.1	±	0.4	-244	±	35	-6	±	11
ID0047	2.615	±	0.025	9.453	±	0.009	2.372	±	0.025	9.458	±	0.008	19.5	±	0.3	-243	±	35	5	±	12
ID0048	3.465	±	0.025	9.642	±	0.011	3.222	±	0.025	9.652	±	0.010	19.2	±	0.4	-243	±	35	10	±	15
ID0049	-0.968	±	0.027	10.156	±	0.007	-1.226	±	0.027	10.138	±	0.007	18.8	±	0.4	-258	±	38	-18	±	10
ID0050	-1.061	±	0.024	9.312	±	0.006	-1.316	±	0.024	9.311	±	0.006	18.2	±	0.4	-255	±	34	—	±	8
ID0051	-1.644	±	0.024	8.968	±	0.007	-1.897	±	0.023	8.956	±	0.007	18.6	±	0.4	-253	±	33	-12	±	10
ID0052	-5.516	±	0.031	11.827	±	0.016	-5.800	±	0.031	11.769	±	0.017	19.8	±	0.7	-284	±	44	-58	±	23
ID0053	-4.664	±	0.030	11.306	±	0.014	-4.940	±	0.030	11.301	±	0.015	19.5	±	0.3	-276	±	42	-5	±	21
ID0054	-8.807	±	0.033	12.330	±	0.024	-9.122	±	0.033	12.337	±	0.025	18.8	±	0.5	-315	±	47	7	±	35
ID0055	-12.998	±	0.034	12.774	±	0.035	-13.254	±	0.034	12.739	±	0.035	19.3	±	0.6	-256	±	48	-35	±	49

Table D.2. continued.

ID	$\Delta\alpha$["]			$\Delta\delta$["]			$\Delta\alpha$["]			$\Delta\delta$["]			K_s [mag]			$\delta\Delta\alpha$[mas]			$\delta\Delta\delta$[mas]		
ID0056	-13.804	±	0.033	12.147	±	0.037	-14.088	±	0.033	12.130	±	0.038	18.4	±	0.5	-284	±	47	-17	±	53
ID0057	-14.100	±	0.031	11.487	±	0.038	-14.349	±	0.031	11.426	±	0.038	19.4	±	0.6	-249	±	44	-61	±	54
ID0058	-15.891	±	0.024	8.285	±	0.042	-16.159	±	0.024	8.268	±	0.043	15.2	±	0.5	-268	±	34	-17	±	60
ID0059	-7.046	±	0.026	9.665	±	0.019	-7.302	±	0.026	9.656	±	0.020	17.4	±	0.4	-256	±	37	-9	±	28
ID0060	-7.789	±	0.029	10.781	±	0.021	-8.055	±	0.029	10.749	±	0.022	19.6	±	0.6	-266	±	41	-32	±	30
ID0061	-8.341	±	0.029	10.856	±	0.023	-8.635	±	0.029	10.842	±	0.023	20.9	±	0.5	-294	±	41	-14	±	33
ID0062	-6.989	±	0.023	8.738	±	0.019	-7.252	±	0.023	8.722	±	0.020	20.0	±	0.9[d]	-263	±	33	-16	±	28
ID0063	-6.684	±	0.019	7.250	±	0.018	-6.953	±	0.019	7.229	±	0.019	19.0	±	0.4	-269	±	27	-21	±	26
ID0064	-4.377	±	0.018	6.647	±	0.012	-4.627	±	0.018	6.640	±	0.013	17.9	±	0.5	-250	±	25	-7	±	18
ID0065	-4.525	±	0.016	6.039	±	0.012	-4.772	±	0.016	6.032	±	0.013	17.0	±	0.4	-247	±	23	-7	±	18
ID0066	-4.525	±	0.016	6.039	±	0.012	-4.772	±	0.016	6.032	±	0.013	17.0	±	0.4	-247	±	23	-7	±	18
ID0067	-1.017	±	0.021	7.835	±	0.005	-1.246	±	0.020	7.816	±	0.006	18.4	±	1.5[a]	-229	±	29	-19	±	8
ID0068	-1.637	±	0.019	7.295	±	0.006	-1.880	±	0.019	7.282	±	0.007	18.6	±	0.5	-243	±	27	-13	±	9
ID0069	-1.399	±	0.015	5.886	±	0.005	-1.636	±	0.015	5.869	±	0.005	18.2	±	0.4	-237	±	21	-17	±	7
ID0070	0.403	±	0.021	7.970	±	0.005	0.159	±	0.021	7.961	±	0.005	17.0	±	0.3	-244	±	30	-9	±	7
ID0071	-12.492	±	0.026	9.687	±	0.033	-12.776	±	0.027	9.731	±	0.034	20.1	±	0.4	-284	±	37	44	±	47
ID0072	-11.868	±	0.022	7.887	±	0.031	-12.115	±	0.022	7.863	±	0.032	19.6	±	0.4	-247	±	31	-24	±	45
ID0073	-12.086	±	0.018	6.158	±	0.032	-12.353	±	0.018	6.133	±	0.033	17.9	±	0.5	-267	±	25	-25	±	46
ID0074	-12.515	±	0.019	6.636	±	0.033	-12.817	±	0.019	6.630	±	0.034	20.0	±	0.8[d]	-302	±	27	-6	±	47
ID0075	-11.278	±	0.018	6.521	±	0.030	-11.558	±	0.018	6.522	±	0.030	19.1	±	0.4	-280	±	25	1	±	42
ID0076	-9.094	±	0.020	7.428	±	0.024	-9.368	±	0.020	7.472	±	0.025	19.5	±	0.4	-274	±	28	44	±	35
ID0077	-8.837	±	0.019	7.130	±	0.023	-9.111	±	0.019	7.008	±	0.024	19.7	±	0.4	-274	±	27	-122	±	33
ID0078	-13.843	±	0.019	6.393	±	0.036	-14.117	±	0.019	6.363	±	0.037	19.2	±	0.7	-274	±	27	-30	±	52
ID0079	-12.928	±	0.013	4.072	±	0.034	-13.151	±	0.013	4.010	±	0.035	20.0	±	0.5	-223	±	18	-62	±	49
ID0080	-13.304	±	0.013	4.143	±	0.035	-13.535	±	0.013	4.117	±	0.036	19.5	±	0.4	-231	±	18	-26	±	50
ID0081	-13.845	±	0.014	4.111	±	0.036	-14.116	±	0.014	4.072	±	0.037	18.9	±	0.7	-271	±	20	-39	±	52
ID0082	-3.875	±	0.008	2.857	±	0.010	-4.086	±	0.008	2.951	±	0.011	17.1	±	0.4	-211	±	11	94	±	15
ID0083	-4.401	±	0.010	3.594	±	0.012	-4.649	±	0.010	3.580	±	0.012	19.8	±	0.7	-248	±	14	-14	±	17
ID0084	-4.962	±	0.010	3.546	±	0.013	-5.218	±	0.010	3.523	±	0.014	18.1	±	0.4	-256	±	14	-23	±	19
ID0085	-5.102	±	0.010	3.747	±	0.014	-5.362	±	0.010	3.724	±	0.014	18.8	±	0.5	-260	±	14	-23	±	20
ID0086	-3.561	±	0.012	4.340	±	0.010	-3.809	±	0.012	4.340	±	0.010	19.5	±	0.3	-248	±	17	0	±	14
ID0087	-5.510	±	0.013	4.835	±	0.015	-5.763	±	0.013	4.822	±	0.015	18.5	±	0.3	-253	±	18	-13	±	21
ID0088	-10.682	±	0.007	-1.022	±	0.028	-10.935	±	0.007	-1.060	±	0.029	17.4	±	0.5	-253	±	10	-38	±	40
ID0089	-11.034	±	0.007	-0.490	±	0.029	-11.289	±	0.007	-0.505	±	0.030	19.5	±	0.3	-255	±	10	-15	±	42
ID0090	-7.401	±	0.006	-1.589	±	0.019	-7.647	±	0.006	-1.620	±	0.020	17.1	±	0.4	-246	±	8	-31	±	28
ID0091	-7.058	±	0.007	-2.340	±	0.019	-7.304	±	0.008	-2.367	±	0.019	17.2	±	0.3	-246	±	11	-27	±	27
ID0092	-8.906	±	0.008	2.189	±	0.023	-9.174	±	0.008	2.131	±	0.024	22.4	±	1.8[a,d]	-268	±	11	-58	±	33
ID0093	-11.528	±	0.009	2.211	±	0.030	-11.819	±	0.009	2.199	±	0.031	19.5	±	0.4	-291	±	13	-12	±	43
ID0094	1.450	±	0.015	5.663	±	0.005	1.209	±	0.015	5.651	±	0.005	19.2	±	0.7	-241	±	21	-12	±	7
ID0095	1.188	±	0.014	5.164	±	0.004	0.925	±	0.013	5.152	±	0.004	18.4	±	0.5	-263	±	19	-12	±	6
ID0096	1.571	±	0.013	5.052	±	0.005	1.333	±	0.013	5.030	±	0.005	18.8	±	0.3	-238	±	18	-22	±	7
ID0097	1.897	±	0.013	4.968	±	0.006	1.655	±	0.013	4.965	±	0.005	17.9	±	0.3	-242	±	18	-3	±	8
ID0098	1.885	±	0.012	4.628	±	0.006	1.644	±	0.012	4.631	±	0.005	18.4	±	0.4	-241	±	17	3	±	8
ID0099	4.854	±	0.024	9.288	±	0.014	4.619	±	0.024	9.288	±	0.013	19.0	±	0.5	-235	±	34	0	±	19
ID0100	4.326	±	0.021	7.897	±	0.012	4.068	±	0.021	7.903	±	0.012	19.5	±	0.5	-258	±	30	6	±	17
ID0101	8.097	±	0.024	8.856	±	0.022	7.867	±	0.023	8.808	±	0.021	22.0	±	0.7	-230	±	33	-48	±	30
ID0102	10.651	±	0.022	8.107	±	0.028	10.427	±	0.022	8.128	±	0.028	18.1	±	0.4	-224	±	31	21	±	40
ID0103	7.372	±	0.016	5.737	±	0.020	7.136	±	0.016	5.740	±	0.019	14.0	±	0.4	-236	±	23	3	±	28
ID0104	6.457	±	0.014	5.051	±	0.017	6.228	±	0.014	5.043	±	0.017	17.9	±	0.3	-229	±	20	-8	±	24

Table D.2. continued.

ID	$\Delta\alpha$["]			$\Delta\delta$["]			$\Delta\alpha$["]			$\Delta\delta$["]			K_s [mag]			$\delta\Delta\alpha$[mas]			$\delta\Delta\delta$[mas]		
ID0105	6.426	±	0.012	4.379	±	0.017	6.192	±	0.012	4.389	±	0.016	13.8	±	0.3	-234	±	17	10	±	23
ID0106	4.477	±	0.011	4.009	±	0.012	4.237	±	0.011	4.006	±	0.011	19.3	±	0.4	-240	±	16	-3	±	16
ID0107	8.397	±	0.010	3.350	±	0.022	8.181	±	0.010	3.356	±	0.022	19.0	±	0.5	-216	±	14	6	±	31
ID0108	8.364	±	0.006	1.566	±	0.022	8.141	±	0.006	1.563	±	0.021	18.5	±	0.3	-223	±	8	-3	±	30
ID0109	11.177	±	0.008	1.725	±	0.029	10.972	±	0.008	1.729	±	0.029	19.5	±	1.2[a]	-205	±	11	4	±	41
ID0110	6.199	±	0.005	1.517	±	0.016	5.972	±	0.005	1.458	±	0.016	18.0	±	0.6	-227	±	7	-59	±	23
ID0111	7.798	±	0.006	-1.437	±	0.020	7.570	±	0.006	-1.443	±	0.020	16.6	±	0.3	-228	±	8	-6	±	28
ID0112	9.992	±	0.007	-1.069	±	0.026	9.774	±	0.006	-1.074	±	0.026	17.6	±	0.4	-218	±	9	-5	±	37
ID0113	10.644	±	0.007	-1.060	±	0.028	10.412	±	0.007	-1.080	±	0.027	19.4	±	1.0[a,d]	-232	±	10	-20	±	39
ID0114	10.654	±	0.007	-0.774	±	0.028	10.433	±	0.007	-0.780	±	0.027	18.2	±	0.3	-221	±	10	-6	±	39
ID0115	4.980	±	0.007	-2.438	±	0.013	4.758	±	0.007	-2.457	±	0.013	19.0	±	0.3	-222	±	10	-19	±	18
ID0116	9.866	±	0.010	-2.898	±	0.026	9.640	±	0.010	-2.901	±	0.025	18.5	±	0.3	-226	±	14	-3	±	36
ID0117	9.696	±	0.010	-3.045	±	0.025	9.480	±	0.010	-3.045	±	0.025	17.4	±	0.3	-216	±	14	0	±	35
ID0118	8.358	±	0.012	-4.031	±	0.022	8.132	±	0.012	-4.039	±	0.021	16.5	±	0.3	-226	±	17	-8	±	30
ID0119	8.940	±	0.013	-4.545	±	0.024	8.720	±	0.013	-4.560	±	0.023	17.6	±	0.4	-220	±	18	-15	±	33
ID0120	9.528	±	0.015	-5.240	±	0.025	9.311	±	0.015	-5.260	±	0.025	19.5	±	0.3	-217	±	21	-20	±	35
ID0121	9.333	±	0.014	-5.014	±	0.025	9.121	±	0.014	-5.029	±	0.024	19.0	±	0.3	-212	±	20	-15	±	35
ID0122	10.977	±	0.018	-6.303	±	0.029	10.764	±	0.018	-6.327	±	0.028	18.0	±	0.5	-213	±	25	-24	±	40
ID0123	10.231	±	0.018	-6.534	±	0.027	10.012	±	0.018	-6.550	±	0.026	16.9	±	0.4	-219	±	25	-16	±	37
ID0124	10.000	±	0.019	-6.989	±	0.026	9.786	±	0.019	-7.007	±	0.026	17.3	±	0.4	-214	±	27	-18	±	37
ID0125	9.228	±	0.017	-5.959	±	0.024	9.011	±	0.017	-5.974	±	0.024	17.1	±	0.3	-217	±	24	-15	±	34
ID0126	7.641	±	0.024	-9.017	±	0.021	7.425	±	0.024	-9.048	±	0.020	17.9	±	0.4	-216	±	34	-31	±	29
ID0127	7.916	±	0.022	-8.255	±	0.021	7.704	±	0.022	-8.274	±	0.021	19.2	±	0.3	-212	±	31	-19	±	30
ID0128	7.315	±	0.020	-7.610	±	0.020	7.088	±	0.020	-7.621	±	0.019	19.2	±	0.3	-227	±	28	-11	±	28
ID0129	6.573	±	0.025	-9.555	±	0.018	6.357	±	0.025	-9.580	±	0.018	19.5	±	0.4	-216	±	35	-25	±	25
ID0130	5.174	±	0.023	-8.561	±	0.014	4.966	±	0.023	-8.578	±	0.014	19.3	±	0.3	-208	±	33	-17	±	20
ID0131	5.090	±	0.022	-8.221	±	0.014	4.863	±	0.022	-8.240	±	0.014	18.9	±	0.3	-227	±	31	-19	±	20
ID0132	4.854	±	0.021	-7.864	±	0.014	4.647	±	0.021	-7.903	±	0.013	19.8	±	0.6	-207	±	30	-39	±	19
ID0133	4.921	±	0.019	-7.214	±	0.014	4.691	±	0.019	-7.216	±	0.013	19.5	±	0.3	-230	±	27	-2	±	19
ID0134	6.189	±	0.014	-5.245	±	0.016	5.973	±	0.014	-5.272	±	0.016	18.9	±	0.3	-216	±	20	-27	±	23
ID0135	5.003	±	0.003	-0.052	±	0.013	4.759	±	0.003	-0.075	±	0.012	19.5	±	0.4	-244	±	4	-23	±	18
ID0136	1.442	±	0.018	-6.727	±	0.005	1.208	±	0.018	-6.776	±	0.005	19.1	±	0.7	-234	±	25	-49	±	7
ID0137	1.217	±	0.017	-6.560	±	0.005	0.982	±	0.017	-6.580	±	0.005	22.1	±	2.1[a,d]	-235	±	24	-20	±	7
ID0138	0.147	±	0.015	-5.920	±	0.004	-0.079	±	0.016	-5.950	±	0.004	18.4	±	0.5	-226	±	22	-30	±	6
ID0139	-1.573	±	0.019	-7.348	±	0.006	-1.785	±	0.019	-7.386	±	0.006	19.0	±	0.5	-212	±	27	-38	±	8
ID0140	-2.515	±	0.022	-8.293	±	0.008	-2.743	±	0.022	-8.327	±	0.009	18.4	±	0.3	-228	±	31	-34	±	12
ID0141	-3.150	±	0.024	-9.116	±	0.010	-3.391	±	0.024	-9.158	±	0.010	19.0	±	0.4	-241	±	34	-42	±	14
ID0142	-2.760	±	0.019	-7.169	±	0.008	-2.989	±	0.019	-7.207	±	0.009	14.6	±	0.3	-229	±	27	-38	±	12
ID0143	-4.665	±	0.017	-6.336	±	0.013	-4.901	±	0.017	-6.363	±	0.013	18.7	±	0.4	-236	±	24	-27	±	18
ID0144	-3.964	±	0.016	-6.069	±	0.011	-4.186	±	0.016	-6.067	±	0.012	19.8	±	0.3	-222	±	23	2	±	16
ID0145	-5.291	±	0.019	-7.130	±	0.014	-5.520	±	0.019	-7.151	±	0.015	20.0	±	0.3	-229	±	27	-21	±	21
ID0146	-5.354	±	0.015	-5.633	±	0.014	-5.606	±	0.015	-5.661	±	0.015	17.2	±	0.3	-252	±	21	-28	±	21
ID0147	-5.459	±	0.012	-4.415	±	0.015	-5.702	±	0.012	-4.441	±	0.015	17.2	±	0.3	-243	±	17	-26	±	21
ID0148	-5.068	±	0.011	-3.964	±	0.013	-5.297	±	0.011	-3.989	±	0.014	19.7	±	0.4	-229	±	16	-25	±	19
ID0149	-6.688	±	0.015	-5.706	±	0.018	-6.925	±	0.016	-5.743	±	0.018	19.7	±	0.8[a,d]	-237	±	22	-37	±	25
ID0150	-8.104	±	0.015	-5.406	±	0.021	-8.336	±	0.015	-5.452	±	0.022	18.8	±	0.4	-232	±	21	-46	±	30
ID0151	-10.863	±	0.022	-7.955	±	0.029	-11.105	±	0.022	-8.008	±	0.029	18.6	±	0.4	-242	±	31	-53	±	41
ID0152	-10.940	±	0.018	-6.415	±	0.029	-11.195	±	0.018	-6.466	±	0.030	19.4	±	0.5	-255	±	25	-51	±	42
ID0153	-10.961	±	0.016	-5.556	±	0.029	-11.207	±	0.016	-5.595	±	0.030	19.3	±	0.3	-246	±	23	-39	±	42

Table D.2. continued.

ID	$\Delta\alpha$["]			$\Delta\delta$["]			$\Delta\alpha$["]			$\Delta\delta$["]			K_s [mag]			$\delta\Delta\alpha$[mas]			$\delta\Delta\delta$[mas]		
ID0154	-12.309	±	0.014	-4.657	±	0.032	-12.561	±	0.014	-4.687	±	0.033	18.6	±	0.5	-252	±	20	-30	±	46
ID0155	-13.460	±	0.014	-4.197	±	0.035	-13.710	±	0.014	-4.235	±	0.036	18.1	±	0.5	-250	±	20	-38	±	50
ID0156	-14.947	±	0.014	-4.246	±	0.039	-15.213	±	0.014	-4.284	±	0.040	19.5	±	0.6	-266	±	20	-38	±	56
ID0157	-14.638	±	0.016	-4.995	±	0.038	-14.886	±	0.016	-5.029	±	0.039	18.4	±	0.4	-248	±	23	-34	±	54
ID0158	-12.859	±	0.012	-3.316	±	0.034	-13.115	±	0.012	-3.348	±	0.034	18.2	±	0.3	-256	±	17	-32	±	48
ID0159	-10.131	±	0.010	-2.930	±	0.027	-10.395	±	0.010	-2.905	±	0.027	19.6	±	0.3	-264	±	14	25	±	38
ID0160	-3.122	±	0.016	-5.979	±	0.009	-3.332	±	0.016	-6.042	±	0.009	17.9	±	0.5	-210	±	23	-63	±	13
ID0161	9.903	±	0.012	-3.896	±	0.026	9.687	±	0.012	-3.908	±	0.025	19.0	±	0.3	-216	±	17	-12	±	36
ID0162	0.333	±	0.009	-3.306	±	0.002	...			...			18.5	±	0.3	...			...		
ID0163	3.099	±	0.003	-0.813	±	0.008	...			...			17.9	±	0.3	...			...		
HD 175742	2004-07-30						2006-06-27														
ID0001	-7.334	±	0.016	5.982	±	0.019	-7.641	±	0.018	6.505	±	0.020	16.5	±	0.5	-307	±	24	523	±	28
ID0003	-3.055	±	0.018	6.934	±	0.009	-3.358	±	0.020	7.474	±	0.010	18.9	±	0.5	-303	±	27	540	±	13
ID0004	2.678	±	0.002	0.050	±	0.007	2.409	±	0.002	0.586	±	0.006	15.9	±	0.3	-269	±	3	536	±	9
ID0005	9.109	±	0.010	-3.397	±	0.024	8.852	±	0.009	-2.859	±	0.023	18.9	±	0.4	-257	±	13	538	±	33
ID0006	-3.039	±	0.023	-8.884	±	0.010	-3.313	±	0.022	-8.375	±	0.010	16.8	±	0.4	-274	±	32	509	±	14
ID0007	...			...			8.801	±	0.046	17.394	±	0.025	18.0	±	0.3	...			...		
ID0008	...			...			3.383	±	0.042	16.147	±	0.013	18.5	±	0.3	...			...		
ID0009	...			...			-2.847	±	0.021	7.972	±	0.009	19.7	±	0.3	...			...		
ID0010	...			...			3.063	±	0.012	4.392	±	0.008	18.9	±	0.3	...			...		
ID0011	...			...			2.610	±	0.024	9.054	±	0.009	20.0	±	0.3	...			...		
ID0012	...			...			-8.037	±	0.045	17.125	±	0.023	19.9	±	0.3	...			...		
ID0013	...			...			-11.710	±	0.010	-2.498	±	0.031	19.5	±	0.3	...			...		
ID0014	...			...			-3.767	±	0.019	-7.102	±	0.011	19.4	±	0.3	...			...		
HIP 104383	2003-11-07																				
ID0001	-10.192	±	0.046	17.479	±	0.029	...			...			16.2	±	0.3	...			...		
ID0002	0.401	±	0.034	12.871	±	0.008	...			...			17.5	±	0.3	...			...		
ID0003	-16.661	±	0.039	14.241	±	0.044	...			...			16.5	±	0.3	...			...		
ID0004	-4.384	±	0.003	-0.608	±	0.011	...			...			17.8	±	0.3	...			...		
ID0005	-4.876	±	0.003	-0.504	±	0.013	...			...			15.7	±	0.3	...			...		

Notes. A list of unique sequential identifiers (prefix 'ID') has been assigned to the candidates **(1)** (cf. Figs. C.1-C.5). For each candidate, the separation from the central star in right ascension and declination is given for the first epoch **(2, 3)** and the second epoch when present **(4, 5)**. Finally, apparent K_s magnitude is given for all candidates **(6)** and - when two epochs are available - the change of separation **(7,8)**. The change in separation reflects the stellar parallactic and proper motion since all candidates are background stars (see text and Table E.2). Large error bars in the magnitude measurement are ascribed to different causes. Those are indicated by letters to the column for error bars $\geq$ 0.8: $^{(a)}$ affected by background features (like diffraction spikes, ghosts, reflections) $^{(b)}$ smeared in first epoch $^{(c)}$ aperture photometry misses flux at edge of frame $^{(d)}$ measurement affected by noise in first epoch.

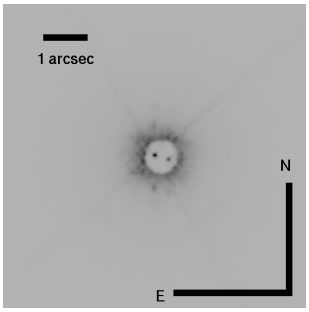

Fig. D.1. The visual binary HIP 104383 A below the semi-transparent coronagraphic mask. The binary has already been characterised (Balega et al. 2004). The full frame exposing companion candidates is shown in Fig. C.4. The magnitudes of the binary components differ by 0.45 mag in the K_s band.

Appendix E: Detection limits

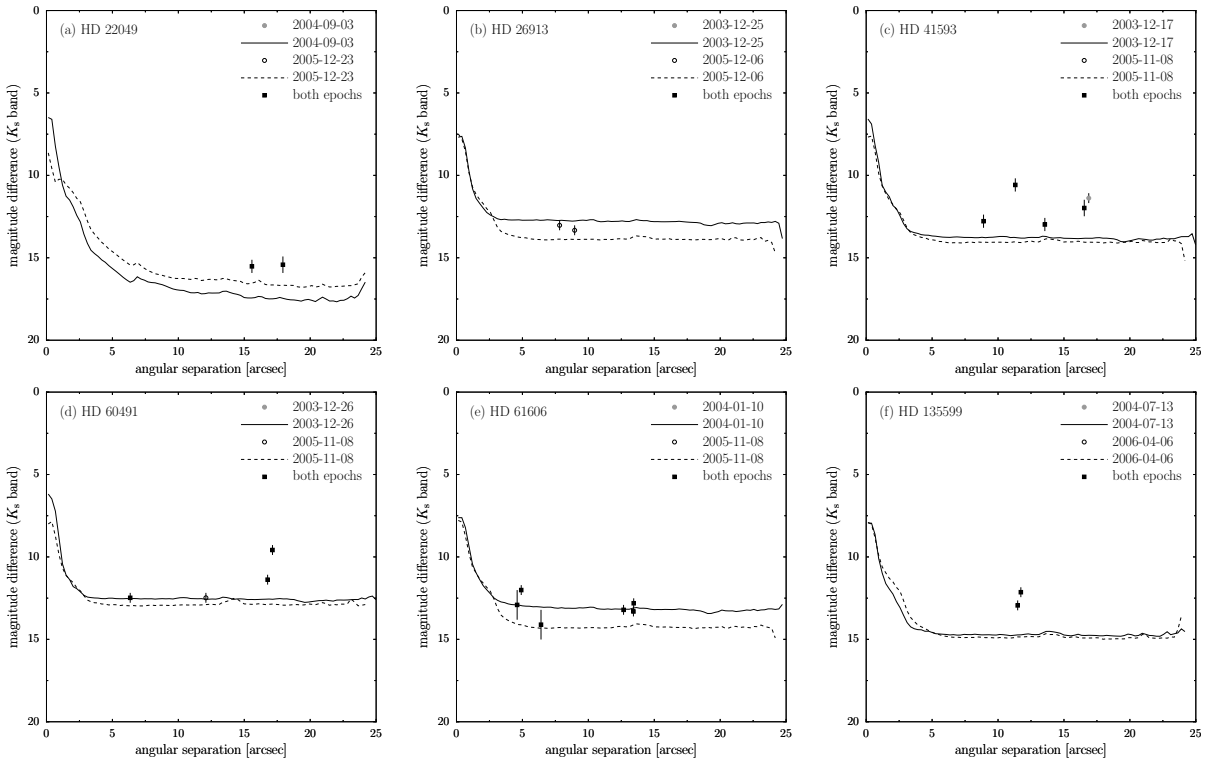

Fig. E.1. Dynamic range curves are shown for stars with candidates and observations in two epochs: HD 22049, HD 26913, HD 41593, HD 60491, HD 61606, and HD 135599. The lines show the $10\,\sigma$ detection limits for the 1st and 2nd epoch as is indicated in the legend. The adoption of a $5\,\sigma$ limit to describe the visual detection of candidates would lower the curves by $2.5 \log 2 = 0.75$ mag. Furthermore, the curves can vary by 0.3 mag due to the uncertainty of the transmission of the coronagraph. Filled circles indicate candidates found in the 1st epoch, open circles those in the 2nd epoch, and filled squares those seen in both epochs.

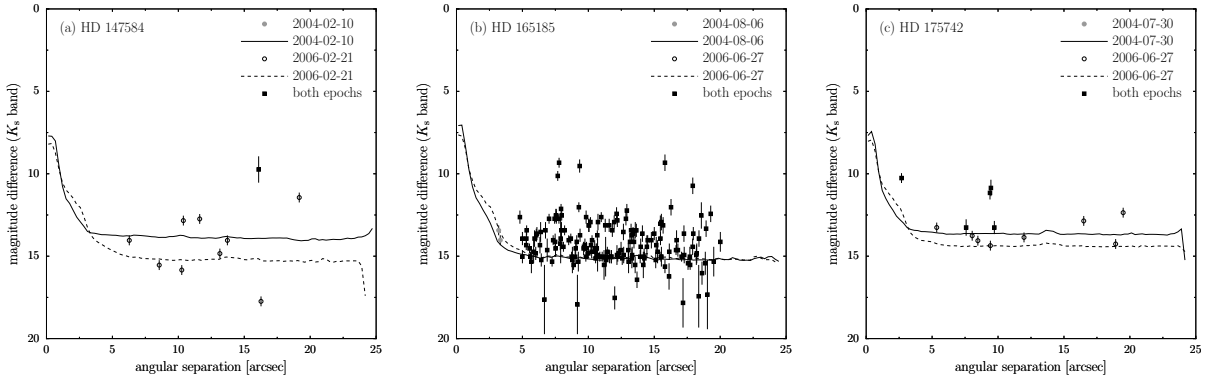

Fig. E.2. Similar to Fig. E.1 for HD 147584, HD 165185, and HD 175742. Some data points are below the detection limits owing to unreliable magnitude measurements (discussed in the text).

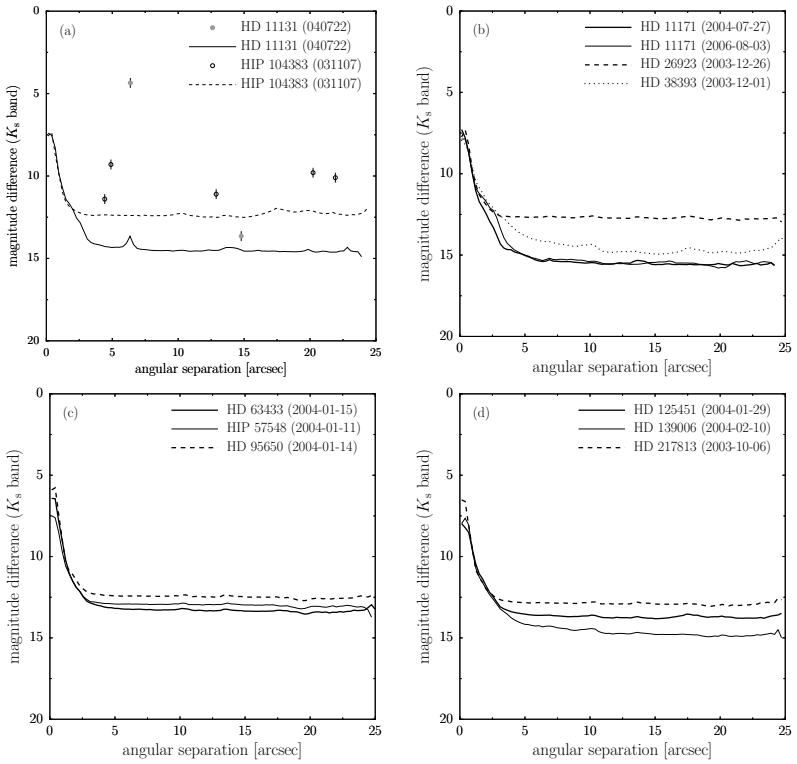

Fig. E.3. Dynamic range curves are shown for stars with candidates detected in a single epoch (HD 11131 and HIP 104383) and for all the other stars without any candidates.

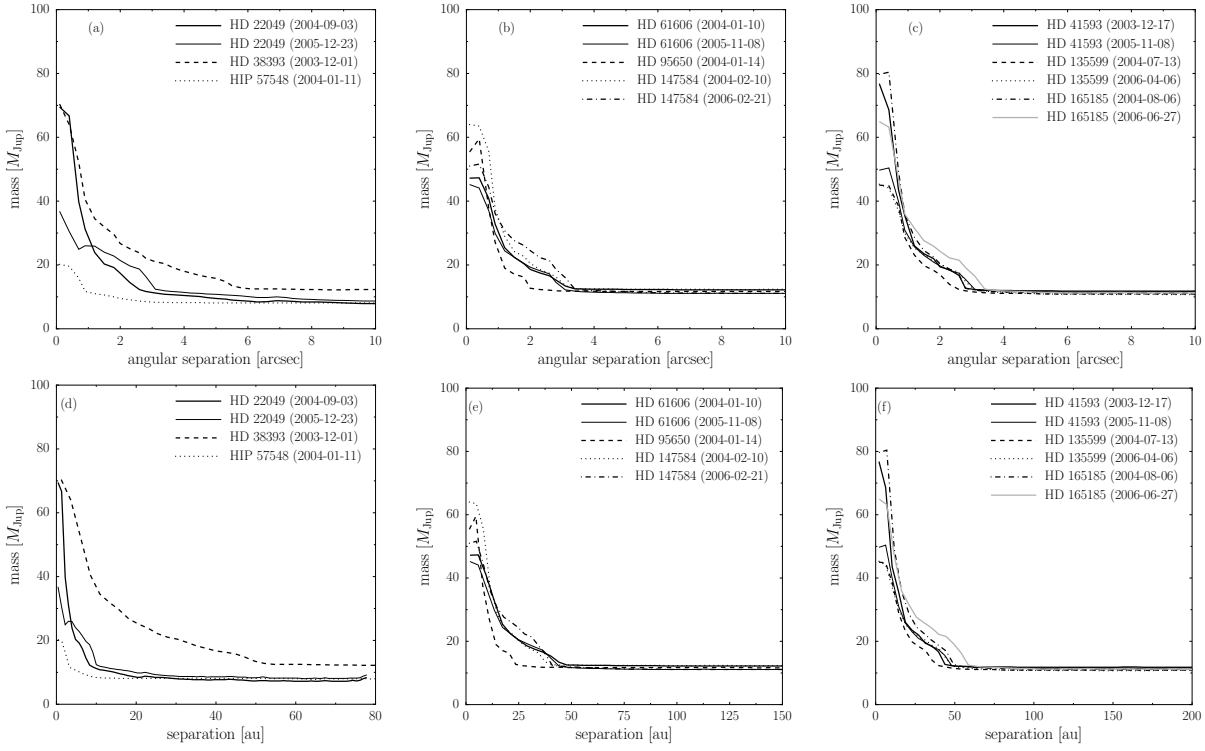

Fig. E.4. Top row: detection limits on mass as a function of angular separation. Bottom row: the same as a function of separation in linear scale (bottom row). Based on the dynamic range curves presented in Figs. 2 and E.1-E.3 and on evolutionary models (DUSTY00 and COND03) assuming an age of 500 Myr. The layout follows Figs. E.3 b, c, and d.

Table E.1. Detection limits derived from exposures of different epochs.

star	epoch	exp. time on target [s]	min. separation [au]								
			12 $M_{\rm Jup}$			20 $M_{\rm Jup}$			35 $M_{\rm Jup}$		
			100 Myr	500 Myr	1 Gyr	100 Myr	500 Myr	1 Gyr	100 Myr	500 Myr	1 Gyr
HD 11131	2004-07-22	720	20.8	86.7	...	17.6	50.7	96.7	<3.2	22.3	34.8
HD 11171	2004-07-27	495	27.0	182.1	...	22.5	63.9	220.8	14.8	29.3	50.3
HD 11171	2006-08-03	1680	27.7	247.7	...	22.5	75.5	255.5	14.5	32.9	66.2
HD 22049[a]	2004-09-03	2475	2.4	8.7	18.4	1.9	5.0	8.8	<0.4	2.6	3.8
HD 22049	2005-12-23	720	<0.4	10.7	29.1	<0.4	7.2	10.8	<0.4	0.7	4.4
HD 26913	2003-12-25	864	17.1	515.8	...	13.8	40.4	516.3	<2.8	18.6	27.2
HD 26913	2005-12-06	630	16.4	97.0	...	12.3	45.5	112.0	<2.8	18.0	29.1
HD 26923	2003-12-26	630	19.0	...	...	16.0	52.1	...	<2.9	20.7	33.2
HD 38393[b]	2003-12-01	1673	9.6	96.4	...	7.5	31.1	97.8	<1.2	10.6	21.0
HD 41593[c]	2003-12-17	1260	13.3	60.9	...	10.2	30.2	65.5	3.1	14.7	20.7
HD 41593	2005-11-08	630	11.4	53.8	...	8.3	30.1	56.2	<2.1	12.6	20.0
HD 60491[d]	2003-12-26	1855	23.0	...	...	19.7	45.7	...	10.1	24.5	32.0
HD 60491	2005-11-08	560	16.5	...	...	10.5	48.8	...	<3.3	18.8	29.7
HD 61606	2004-01-10	560	11.0	345.3	...	7.2	25.6	344.3	<1.9	12.2	18.0
HD 61606	2005-11-08	630	9.1	45.6	...	4.1	26.4	46.3	<1.9	10.5	16.9
HD 63433	2004-01-15	980	21.4	...	...	17.6	46.5	...	11.1	23.2	33.2
HIP 57548	2004-01-11	630	<0.5	2.9	8.2	<0.5	0.7	3.0	<0.5	<0.5	<0.5
HD 95650	2004-01-14	630	7.9	30.9	...	6.4	13.7	32.3	<1.6	8.6	11.8
HD 125451	2004-01-29	630	31.7	...	...	25.7	91.0	...	10.4	35.8	63.7
HD 135599[e]	2004-07-13	1080	10.8	43.0	...	6.4	22.8	43.7	<2.1	11.9	17.5
HD 135599	2006-04-06	1680	10.0	49.8	...	4.6	32.2	50.5	<2.1	11.6	19.7
HD 139006	2004-02-10	620	52.2	...	...	39.3	...	...	24.7	60.4	140.0
HD 147584	2004-02-10	665	11.4	...	...	9.7	25.3	...	<1.6	12.4	17.5
HD 147584	2006-02-21	630	10.7	47.4	292.1	8.1	32.7	49.3	<1.6	12.0	23.7
HD 165185[f]	2004-08-06	810	15.5	54.6	...	13.0	36.2	56.1	7.8	16.8	25.3
HD 165185	2006-06-27	1680	15.4	65.5	...	12.5	47.4	67.2	<2.3	17.2	33.6
HD 175742	2004-07-30	540	16.4	77.5	...	12.9	33.1	88.9	<2.9	17.7	24.4
HD 175742	2006-06-27	1680	15.1	70.0	...	9.0	44.8	71.1	<2.9	16.8	26.8
HD 217813[g]	2003-10-06	1146	23.3	...	...	19.5	60.1	...	12.9	25.0	39.3
HIP 104383	2003-11-07	630	16.5	...	...	12.5	35.5	...	<3.6	18.5	28.3

Notes. (1) Name of the target star. – **(2)** Epoch of exposure (average if several visits have been co-added, see below). – **(3)** On-target exposure time (total exposure time on target if several visits have been co-added). – **(4-12)** lower limit on the separation of detectable objects for masses of 12, 20, and 35 $M_{\rm Jup}$ and ages of 100 Myr, 500 Myr, and 1 Gyr, respectively. The relation of masses and magnitudes has been interpolated in the DUSTY00 and COND03 grids. Several targets have been observed repeatedly: [(a)] 2, 3, and 5 Sep 2004 [(b)] 4 and 22 Nov 2003 and 4 Jan 2004 [(c)] 22 Nov 2003 and 11 Jan 2004 [(d)] 22 Nov 2003, 10 and 15 Jan 2004 [(e)] 4 and 22 Jul 2004 [(f)] 4 Jul and 9 Sep 2004 [(g)] 6 and 7 Oct 2003.

Table E.2. Apparent motion in right ascension and declination predicted for all stars with at least one candidate observed in two epochs.

star	1st epoch date yyyy mm dd	2nd epoch date yyyy mm dd	$\Delta\alpha\cos\delta$ [mas]	$\Delta\delta$ [mas]
HD 22049	2004-09-03	2005-12-23	-1734.94 ± 0.36	-155.21 ± 0.28
HD 41593	2003-12-17	2005-11-08	-190.06 ± 1.40	-193.41 ± 0.81
HD 60491	2003-12-26	2005-11-08	-128.10 ± 2.43	-72.76 ± 1.25
HD 61606	2004-01-10	2005-11-08	185.25 ± 1.40	-499.95 ± 0.57
HD 135599	2004-07-13	2006-04-06	398.45 ± 1.52	-255.43 ± 1.09
HD 147584	2004-02-10	2006-02-21	410.33 ± 0.51	213.21 ± 0.88
HD 165185	2004-08-06	2006-06-27	234.38 ± 1.17	12.16 ± 0.60
HD 175742	2004-07-30	2006-06-27	276.77 ± 1.05	-537.13 ± 1.20

Notes. Based on proper motion and stellar parallactic motion measured by *Hipparcos* (Tables A.1 and A.2). These numbers are used to identify non-moving background stars next to the targets.

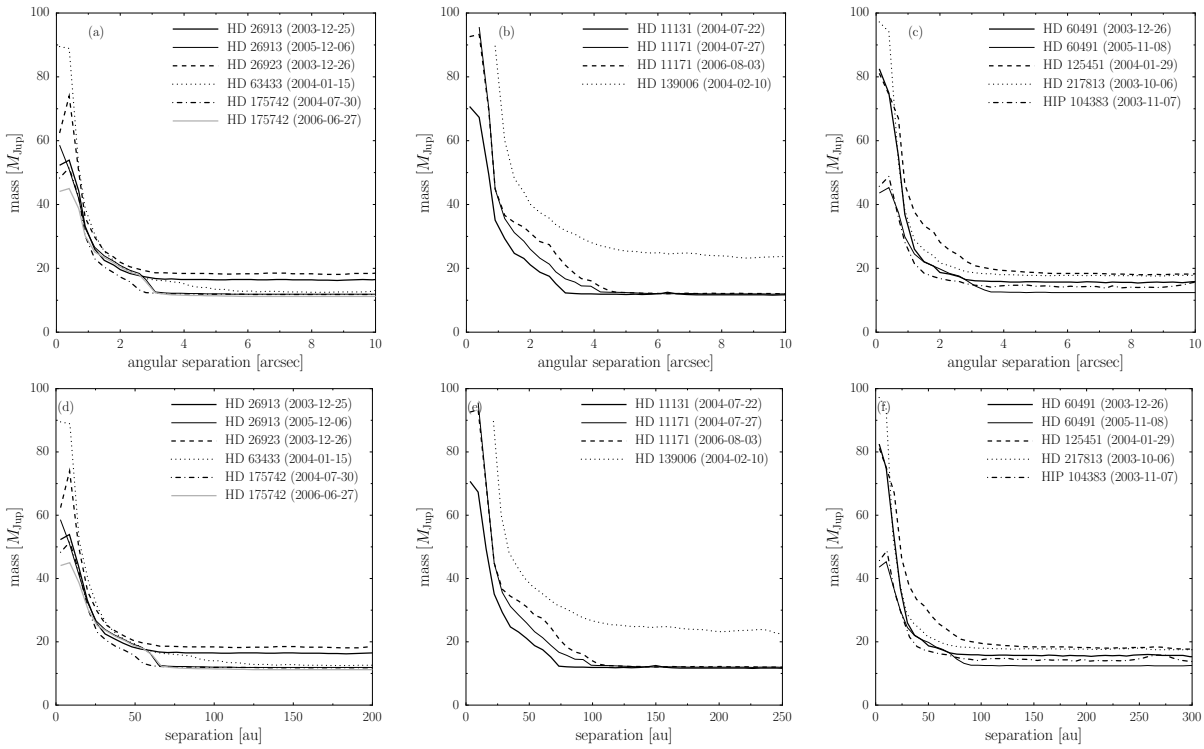

Fig. E.5. Same as in Fig. E.4 for the remaining objects.

1